Some remarks on the abundance of stable periodic orbits inside homoclinic lobes

C. Simó, A. Vieiro
Departament de Matemàtica Aplicada i Anàlisi
Universitat de Barcelona
Gran Via, 585, 08007, Barcelona, Spain

June 27, 2011

Abstract

We consider a family F_ϵ of area-preserving maps (APMs) with a hyperbolic point H_ϵ whose invariant manifolds form a figure-eight and we study the abundance of elliptic periodic orbits visiting homoclinic lobes (EPL), a domain typically dominated by chaotic behavior. To this end, we use the Chirikov separatrix map (SM) as a model of the return to a fundamental domain containing lobes. We obtain an explicit estimate, valid for families F_ϵ with central symmetry and close to an integrable limit, of the relative measure of the set of parameters ϵ for which F_ϵ has EPL trajectories. To get this estimate we look for EPL of the SM with the lowest possible period. The analytical results are complemented with quantitative numerical studies of the following families F_ϵ of APMs:

- The SM family, and we compare our analytical results with the numerical estimates.
- The standard map (STM) family, and we show how the results referring to the SM model apply to the EPL visiting the lobes that the invariant manifolds of the STM hyperbolic fixed point form.
- The conservative Hénon map family, and we estimate the number of a particular type of symmetrical EPL related to the separatrices of the 4-periodic resonant islands.

The results obtained can be seen as the quantitative analogous to those in [17], although here we deal with the *a priori stable* situation instead.

1 Introduction and general background

Let $F_\epsilon : \mathcal{U} \to \mathbb{R}^2$ be a one-parameter family, with $0 < \epsilon << 1$, of real analytic area-preserving maps (APMs, for short) defined on an open domain $\mathcal{U} \subset \mathbb{R}^2$. Assume that the parameter ϵ plays the role of a distance-to-integrable parameter (see [19]). Concretely, consider that for $\epsilon = 0$ the map F_0 is integrable, and that the maps F_ϵ become more chaotic as ϵ increases. Concerning the geometry of F_ϵ we assume that, for $\epsilon > 0$, it has a hyperbolic fixed point H_ϵ, smoothly depending on ϵ, whose stable/unstable invariant manifolds $W^{s/u}(H_\epsilon)$ form a perturbed (conservative) figure-eight, see Fig. 1. To fix ideas, the dynamics on the invariant manifolds of the figure-eight is assumed to be clockwise oriented in all the sketches through the text.

The invariant manifolds of H_ϵ for $\epsilon > 0$ do not coincide and they bound an infinity number of homoclinic lobes (F_ϵ preserves area). Our interest in this work is to provide some quantitative

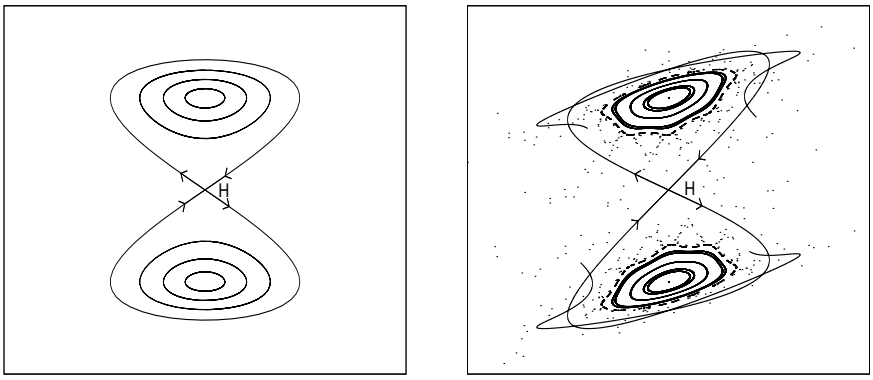

Figure 1: Sketch of an integrable figure-eight (left) and a perturbed one (right). The dynamics along the invariant manifolds is clockwise oriented.

information on the existence of *elliptic periodic orbits visiting the homoclinic lobes* (EPL, for short) created by the invariant manifolds of H_ϵ (see Fig. 1 right). Note that, as ϵ changes, the invariant manifolds move. In particular, each time the manifolds approach to a homoclinic tangency a pair of elliptic-hyperbolic periodic orbits are created. This heuristic argument justifies the existence of EPL.

The EPL trajectories are a particular type of stable motions inside the chaotic region that the homoclinic tangle creates in a generic non-integrable system. Several works deal with the existence and abundance of stable periodic motions inside the chaotic zone. We consider relevant to stress the differences with the present work. For example, the works [10, 14, 13, 11] consider periodically-perturbed $1 + 1/2$ d.o.f. Hamiltonian systems and slow-fast 2 d.o.f. Hamiltonian systems and establish the existence of a set of initial conditions that give rise to stable periodic orbits with passages through the separatrix of the "frozen" system (they deal with the so-called adiabatic approximation of the dynamics). The main conclusion in these works is that the measure of this set of initial conditions remains finite when the system approaches the integrable 1 d.o.f. limit system. Nevertheless, these trajectories are never inside homoclinic lobes. Indeed, in a suitable Poincaré section, these stable periodic trajectories are regular stable periodic orbits that are created as a consequence of the breakdown of a resonant invariant curve, hence being Birkhoff periodic orbits (i.e. well-ordered trajectories of a suitable twist map modelling the dynamics in the region of interest) that appear at some distance from the separatrices (the iterates of a Birkhoff trajectory should avoid the homoclinic lobes). Following [4] we studied the abundance of Birkhoff stable periodic orbits inside the chaotic region in [19], where we concluded that the number of Birkhoff islands of stability inside the chaotic region is $\#\{\text{islands}\} \approx 1.415 \times b$. For an *a priori stable* family of APMs F_ϵ one has $b = \mathcal{O}(1/\epsilon^r)$ with $r > 0$ (see comments in Section 1.2), and hence $\#\{\text{islands}\} \to \infty$ as $\epsilon \to 0$.

In this work we look for EPL, i.e., stable motions inside the figure-eight homoclinic lobes. These EPL trajectories, that exist for some arbitrary $\epsilon > 0$, do not have their equivalent in the integrable map ($\epsilon = 0$) for which the manifolds coincide and there are not homoclinic lobes. They are irregular stable motions [6], that is, these EPL trajectories are not of Birkhoff type and do not appear as a consequence of the breakdown of a resonant invariant curve. While for a Birkhoff periodic orbit the creation-destruction pattern is well-known, not so much is known about the bifurcation (creation-destruction) pattern, the location or the size of the non-Birkhoff EPL trajectories and related stability domains. EPL trajectories have been observed in many

examples and their abundance for near-integrable maps was discussed in [17]. In that paper the authors prove that as $\epsilon \to 0$ the measure of the set of ϵ-parameters for which the map has EPL trajectories is bounded from below. The present work is based on the results in [17].

1.1 The size of the homoclinic lobes and the stability domains related to EPL

An EPL trajectory has all the iterates inside the homoclinic lobes that are generically created by the splitting of separatrices for a non-integrable system. By Moser's twist theorem there exist (generically) rotational invariant curves (of F_ϵ^P) around each iterate of a P-periodic EPL trajectory. These curves bound stability domains inside the homoclinic lobes. The relative size (with respect to the size of the homoclinic lobes) of these stability domains is of the order of the size of the homoclinic lobes (which changes with ϵ). However, for a fixed ϵ, their relative size is expected to be very small [17]. For each family of APMs considered in this work, we show a specific type of EPL trajectories, giving an idea of the relative size of the stability domain surrounding them and how it evolves as ϵ changes.

The size of (and the dynamics inside) the homoclinic lobes for a concrete family F_ϵ depends, in particular, on the hyperbolicity properties of the integrable limit $\epsilon \to 0$ that the family F_ϵ has. Denote by $\lambda(\epsilon)$ the dominant eigenvalue of $DF_\epsilon(H_\epsilon)$. Following the ideas in [3], we distinguish two different situations.

- In the *a priori unstable* situation the map F_0 has a non-degenerate (i.e. $\lambda(0) > 1$ and $\lambda(\epsilon) = \lambda(0) + \mathcal{O}(\epsilon^r)$, $r > 0$) hyperbolic fixed point H_0 whose stable/unstable manifolds $W^{s/u}(H_0)$ form an (integrable) figure-eight (see Fig. 1 left).
- In the *a priori stable* situation, of interest for the purposes of this paper, the hyperbolic fixed point H_ϵ turns out to be degenerated (we encounter, for example, a degenerated invariant curve of fixed points) for $\epsilon = 0$ and, consequently, the map loses hyperbolicity for $\epsilon \to 0$ (see remark below). This situation covers the case of hyperbolic points created when perturbing a resonant curve of an integrable APM (generically, a pair of elliptic-hyperbolic Birkhoff periodic orbits are created, the manifolds of the hyperbolic periodic points surround the elliptic periodic ones forming a pendulum-like structure containing an island of stability) [1]. In particular, we assume that $\lambda(\epsilon) = 1 + \mathcal{O}(\epsilon^r)$, $r > 0$.

Remark. One can also consider an scenario in which the hyperbolic point H_ϵ becomes weakly hyperbolic for $\epsilon = 0$ (i.e. with $\lambda(0) = 1$). As a concrete example, consider the family of APMs $F_\epsilon(x, y) = (\bar{x}, \bar{y}) = (x + (\bar{y} + \nu x)/4, y + (4x^3 - 6x^5 - \epsilon y)/4)$, where $\nu = \epsilon/(4 - \epsilon)$. We are interested in values $|\epsilon| << 1$. The origin is a fixed point and $\mathrm{Spec}(DF(0,0)) = \{\lambda, \lambda^{-1}\}$, with $\lambda = 1 - \epsilon/4$. The points $p_e^\pm = (\pm\sqrt{2/3} \pm \sqrt{3}\epsilon^2/8\sqrt{2} + \mathcal{O}(\epsilon^3), \mp\sqrt{2}\epsilon/\sqrt{3} + \mathcal{O}(\epsilon^2)$ are elliptic points. For $\epsilon \neq 0$ the origin is a (non-degenerated) hyperbolic point whose invariant manifolds surround the points $p_e^\pm$ creating a figure-eight. For $\epsilon = 0$, the origin becomes parabolic with stable/unstable invariant manifolds (locally $y = g(x) = \pm\sqrt{2}x^2 \pm \mathcal{O}(x^3)$) which also form a (perturbed) degenerated figure-eight. We note that for $\epsilon = 0$ the map is not integrable. Instead, one can consider the stroboscopic map related to the vector field defined in terms of a Hamiltonian function of the form $\mathcal{H}(x, y, t) = \mathcal{H}_0(x, y) + \epsilon\mathcal{H}_1(x, y, t/\epsilon)$, with $\mathcal{H}_1$ 2π-periodic in t/ϵ and, for example, $\mathcal{H}_0(x, y) = y^2/2 - x^4 + x^6$ to have a degenerated non-perturbed figure-eight for $\epsilon = 0$. We also note that this situation might behave like the *a priori stable* case (for instance, some exponentially small phenomena

[1] The change of variables that allows to identify the manifolds forming a pendulum-like island with a figure-eight was described in [19]. We briefly recall that, given an APM F in action-angle coordinates (I, φ) having a stability island whose elliptic point is located at $I \approx I_*$, $\varphi = 0$, then the identification to obtain the figure-eight representation maps the elliptic point inside the island to infinity, while the points corresponding to $I = -\infty$ and $I = +\infty$ are mapped to the elliptic points inside the loops of the figure-eight.

might appear [1]) although some weak hiperbolicity remains for the limit map. For simplicity, we do not consider this parabolic weakly-hyperbolic situation although the same techniques could be applied to describe EPL in this setting. We are mainly interested in EPL visiting homoclinic lobes related to the invariant manifolds of (Birkhoff) resonant islands of stability which are created at the breakdown of a resonant rotational invariant curve, hence there is no hyperbolicity, neither of weakly type, for $\epsilon = 0$.

The reader is referred to [19] for a detailed description of both cases. For our purposes, the most relevant difference between the two situations above concerns the size (width) $\mathcal{A}_\epsilon$ of the homoclinic lobes: generically, $\mathcal{A}_\epsilon = \mathcal{O}(\epsilon^r)$, $r > 0$, in the *a priori unstable* case, while it becomes exponentially small with respect to (some power of) ϵ (i.e., $\mathcal{A}_\epsilon = \mathcal{O}(\exp(-c/\epsilon^r))$, with $r, c > 0$ constants) in the *a priori stable* one. Hence, in particular, the problem of finding EPL trajectories becomes much more involved (and the numerical computations become more cumbersome) in the last situation. We stress that:

- The dynamics inside the homoclinic lobes can look like chaotic but the existence of EPL prevent from ergodicity.
- However, the related EPL "islands" of stability, might be very small (and, consequently, hard to be observed in the phase space, see [17]). This explains why it is commonly accepted that the dynamics inside lobes is ergodic, although formally speaking, it is not. Indeed, the dynamics may seem to behave as ergodic, see [12].
- The evolution of the stability domain as ϵ varies follows the general pattern and, in particular, it suffers drastic changes in size when the resonant islands emanate from it (see [16, 18, 20, 19] for a description of this mechanism).
- Islands of stability are sticky because the tiny gaps of the cantori surrounding them are "difficult to cross". In particular, chaotic trajectories stick around islands of stability for relatively long times (see Section 4.1.1 for a numerical study of the stickiness effects).

1.2 General comments on the SM model

To analyze the existence of EPL for F_ϵ we recall that, in a suitable neighborhood of size $\mathcal{O}(\mathcal{A}_\epsilon)$ containing the figure-eight separatrices, the dynamics of F_ϵ can be approximated by the dynamics of the separatrix map model [25, 4], from now on SM for short. The errors of this approximation can be bounded explicitly [15]. The SM becomes in such a way a universal return model that captures the whole dynamics of an APM family F_ϵ in a suitable neighborhood of the figure-eight separatrices. The following comments try to clarify why we can deal with a simple SM model in our theoretical discussions.

- In a concrete problem the figure-eight loops may not necessary be totally symmetric [15, 17] (by totally symmetric we mean that the figure-eight is symmetric with respect to the vertical and horizontal axis, hence, both loops of the figure-eight are equal).
- Accordingly, the proper SM model must take into account the difference between the figure-eight loops. This gives a model, named as *double* SM (DSM from now on) in [19], defined in a fundamental domain which is the union of two annuli (each one captures the dynamics in a neighborhood of one of the two loops). The Chirikov leading approximation of the DSM (see comments below) is given by

$$\text{DSM} : \begin{pmatrix} x \\ y \\ s \end{pmatrix} \longmapsto \begin{pmatrix} \bar{x} \\ \bar{y} \\ \bar{s} \end{pmatrix} = \begin{pmatrix} x + a_{s,\bar{s}} + b \log |\bar{y}| \pmod 1 \\ y + \nu_{\bar{s}} \sin 2\pi x \\ \text{sign}(y)\, s \end{pmatrix}. \tag{1}$$

The parameters $a_{s,\bar{s}}$ are related to the reinjections after the passage close to the hyperbolic point H, the parameter $\nu_{\bar{s}}$ measures the ratio between the inner and outer splittings and the parameter b is defined as for the SM, that is, $b = 1/\log(\lambda)$, being λ the dominant eigenvalue of H. The variable s is equal to 1 (resp. -1) in and around the upper (resp. lower) lobes. See related comments on the parameters of the SM (2) below.

- Under generic assumptions, the figure-eight that form the invariant manifolds of a Birkhoff hyperbolic point of a pendulum-like resonance is non-symmetric and, in particular, the splitting angle of the separatrices in both loops is of different size (see [18]). However, the lack of symmetry is not detected in the first order approximation of the dynamics within the resonance, which is given by a (discrete) pendulum [4, 18].
- In particular, we assume that F_ϵ commutes with the central symmetry Z_ϵ with respect to H_ϵ. This implies that the figure-eight is totally symmetric. One can then identify both annuli where the DSM model is defined and get a much simpler SM model, given by (2) below, defined on a single annulus instead. See [17] for comments on this reduced model.
- The central symmetry property does not hold for a generic family of APMs: it implies an over-simplified dynamics for F_ϵ. This can be specially relevant in non-generic situations. For this reason, we include in Section 4 an analysis of the 1:4 resonant island of the Hénon map as an example of a (completely!) non-symmetric *a priori stable* situation.
- Moreover, in this paper we deal with the so-called Chirikov SM which is a leading explicit approximation to the general Zaslavsky SM. It is obtained assuming that, in the fundamental domain, the oscillation between $W^{u/s}_{\rm loc}(H_\epsilon)$ is sinusoidal (the higher harmonics are ignored). The reasoning in [2] shows that the Chirikov SM is, generically, the suitable model at least in close enough to integrable systems (that is, in an integrable limit sense). Further details can be found in [19].

To sum up, we consider the Chirikov DSM but defined on a totally symmetric figure-eight. If we identify both annuli where the double separatrix map is defined, for $x \in \mathbb{R}/\mathbb{Z}$ and $y \in \mathbb{R}$, the reduced map is given by

$$\mathrm{SM}_{a,b} : \begin{pmatrix} x \\ y \end{pmatrix} \mapsto \begin{pmatrix} x_1 \\ y_1 \end{pmatrix} = \begin{pmatrix} x + a + b\log|y_1| \\ y + \sin(2\pi x) \end{pmatrix}, \tag{2}$$

for suitable parameters a and b (see comments below). To derive the model (2) the y-variable has been rescaled by the size of the splitting, which is assumed to be the same in both loops of the figure eight (recall that the splitting behaves as a power of ϵ or exponentially small in ϵ according to the hyperbolic properties of the integrable limit of F_ϵ, see Section 1.1). We stress the fact that the SM model (2) provides not only qualitative but also quantitative information concerning the dynamics of F_ϵ in a tubular region containing the separatrices.

As observed in [15, 19], the SM (2) is useful to describe the dynamics of F_ϵ in both *a priori stable/unstable* situations. The dynamical differences between these situations are reflected in the parameters a and b, $a, b \in \mathbb{R}$, $b \neq 0$ (of course, a is taken modulus 1) of (2) and, more concretely, on their dependence on the distance-to-integrable parameter ϵ.

The parameters a and b in (2) have a geometrical meaning. Assume that we want to study the dynamics of an APM F around the separatrices emanating from a fixed/periodic hyperbolic point H. Roughly speaking, the parameter a can be seen as a phase shift of the reinjection of the dynamics to the fundamental domain of definition of the model (2). On the other hand, $b = 1/\log(\lambda)$ where λ is the dominant eigenvalue (i.e. $\lambda > 1$) of $DF(H)$. Further details can be found in [2, 15, 17].

If, instead of a single map F, we consider a one parameter family F_ϵ as above, then the parameters a and b in (2) depend on the distance-to-integrable parameter ϵ. Concretely, see [19] and compare with [15], we have the following relation in the *a priori stable/unstable* situations:

$$\begin{aligned} &\textit{a priori unstable} \text{ case:} \quad a = \mathcal{O}(-\log \epsilon) \ , \ b = \mathcal{O}(1), \\ &\textit{a priori stable} \text{ case:} \qquad a = \mathcal{O}(1/\epsilon^{2r}) \quad , \ b = \mathcal{O}(1/\epsilon^r), \end{aligned} \tag{3}$$

where $r > 0$ is such that $\lambda = 1 + \mathcal{O}(\epsilon^r)$. In any case, the value of a has to be taken modulus 1. In particular, in the *a priori unstable* case the parameters a and b can be considered as independent (their first order approximations are independent) while in the *a priori stable* case they depend on each other.

We want to study the existence of EPL in an *a priori stable* family F_ϵ for values of $0 < \epsilon << 1$, that is, for maps F_ϵ close to the integrable map F_0. One has $b(a) \approx \epsilon^r a$ according to (3), hence $b'(a) \approx \epsilon^r \to 0$ as $\epsilon \to 0$ since $r > 0$. Consequently, in a integrable limit sense, both parameters become independent also in the *a priori stable* case. In other words, the value of a changes quickly for $\epsilon \to 0$: a small variation of ϵ produces a change of $\mathcal{O}(1)$ in the value of a.

Concretely, in Section 2, we consider an *a priori stable* family of APMs F_ϵ and we discuss on the limit integrable (that is, $\epsilon \to 0$) of the measure of the set of parameters (a, b) for which one expects to have EPL. To this end, we take the following strategy: we consider b fixed (and large enough because $b = \mathcal{O}(1/\epsilon^r)$) and we compute the set of a values for which one has EPL. A transversality argument, see Section 2.3, rigorously justifies this approach. Naively, one might think that we are considering an *a priori stable* situation like if it was an *a priori unstable* one where a and b are independent each other.

Remark. For $\epsilon \to 0$ (equivalently $b \to \infty$) the number of iterates to return to the fundamental domain where the SM is defined tends to $+\infty$. The size of the fundamental domain (before scaling to get $x \in [0, 1]$ and $y = \mathcal{O}(1)$ in (2), that is, in the original coordinates of F_ϵ) tends to 0 because the dynamics along the invariant manifolds becomes trivial and the distance between consecutive homoclinics tends to 0.

1.3 The type of EPLs under consideration

Consider a family F_ϵ of APMs with a hyperbolic point H_ϵ whose invariant manifolds form a perturbed figure-eight, see Fig. 1 right. The splitting of the separatrices bounding each unperturbed loop of the figure-eight creates a family of homoclinic lobes. Hence, related to a perturbed figure-eight there are two families of homoclinic lobes. An EPL trajectory can visit only the homoclinic lobes of one family or both families of homoclinic lobes. See Fig. 2, left and right respectively, for an illustration of each type of EPL.

In general, by "the period" of a given EPL trajectory $\{x_k\}_{k=1,\dots,P}$ of F_ϵ, and depending on the context, we can refer to the period P of the EPL (i.e. $F_\epsilon^P(x_1) = x_1$), to the period $\hat{p}$ in terms of the DSM model (1), or to the period p in terms of the SM model (2).

Recall that, for the analytical results in this paper, we impose that the F_ϵ commutes with Z_ϵ (the central symmetry with respect to H_ϵ) and, accordingly, we use model (2) to determine EPL trajectories. In this case the simplest EPL have period $p = 2$. An example of an EPL trajectory with period $p = 2$ visiting all the homoclinic lobes and commuting with Z_ϵ is represented in Fig. 2 right. Note that, for such trajectories one has $\hat{p} = 2\,p$, $z_3 = Z_\epsilon(z_1)$ and $z_4 = Z_\epsilon(z_2)$. Period $p = 2$ EPL are expected to be dominant for families commuting with Z_ϵ, i.e., their related islands of stability are expected to be larger.

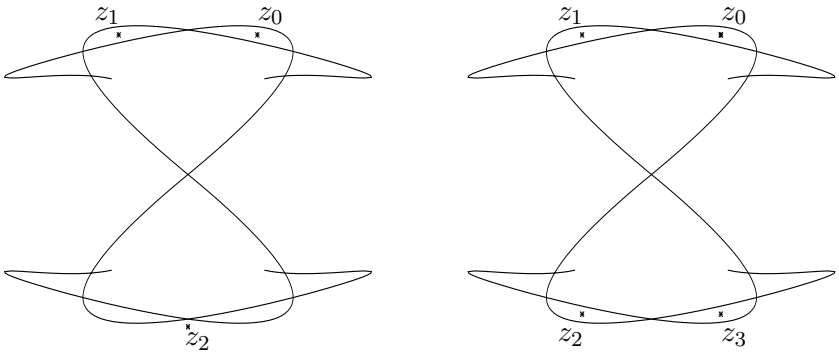

Figure 2: We represent an EPL trajectory of an APM F by the iterates z_i that fall into the fundamental domain where the SM is defined. One has, $z_i = SM^i(z_0)$ (if points are expressed in the suitable SM coordinates). Left: An EPL trajectory of lowest possible period ($\hat{p} = 3$) visiting some homoclinic lobes. It does not visit the lobes of the bottom loop of the figure-eight. This type of orbits where considered in [17]. Right: An EPL trajectory of lowest possible period ($\hat{p} = 4$ or, equivalently, $p = 2$) visiting all the homoclinic lobes. They are dominant if F_ϵ commutes with Z_ϵ. This is the type of orbits we consider through this work.

In [17] the authors considered, for theoretical purposes, period $\hat{p} = 3$ orbits of the DSM. In Fig. 2 left we give an illustration of an orbit of such type. Note that these EPL trajectories do not visit all the homoclinic lobes and that do not respect the central symmetry Z_ϵ (the point $Z_\epsilon(z_2)$ is not a point of the EPL trajectory). Instead, below we consider period $\hat{p} = 4$ orbits which is the lowest possible period for the DSM if the EPL trajectory visits all the lobes (Fig. 2 right).

Remark. In our numerical investigations we deal with symmetric and also non-symmetric families F_ϵ. Accordingly, different types of EPL are considered in each case. However, our analytical results concern period $p = 2$ EPL.

1.4 Brief presentation of the analytical and numerical results of this work

Given a family of APMs F_ϵ as before, denote by $F' = d/d\epsilon|_{\epsilon=0} F_\epsilon$, which is a Hamiltonian vector field, and then $F_\epsilon = F_0 + F'\epsilon + \mathcal{O}(\epsilon^2)$. Denote by $\mathcal{A}$ the set of real analytic vector fields. Using a rigorous derivation of the separatrix map [15], and in the *a priori unstable* context, the following result was proved in [17].

Theorem 1.1 *Let $J(F_\epsilon) \subset (-\epsilon_0, \epsilon_0)$ be the set of values ϵ, with $|\epsilon| < \epsilon_0$ for some fixed small ϵ_0, for which the map F_ϵ has an EPL trajectory. There exists an open set $\mathcal{S} \subset \mathcal{A}$ such that for any $F' \in \mathcal{S}$, the relative measure of $J(F_\epsilon)$ on $(-\epsilon_0, \epsilon_0)$ remains, when $\epsilon_0 \to 0$, greater than a constant $K > 0$ independent of ϵ.*

As detailed in (3), one has $b = \mathcal{O}(1)$ as $\epsilon \to 0$ for an *a priori unstable* family of APMs. Hence, Theorem 1.1 is a consequence of the fact that, for a fixed b, the separatrix map (2) or, more generally, the DSM model if F_ϵ does not commute with the central symmetry, has a set E_b of values of a of positive Lebesgue measure m_L for which the system has EPL.

Note that to get $m_L(E_b)$ involves to consider all types of EPL of any period. A lower bound of $m_L(E_b)$ can be obtained by considering a specific type of EPL of a concrete period. Let $E_b^{\{3\}} \subset E_b$ be the subset of a-parameters for which one has period $\hat{p} = 3$ EPL, like the one shown in Fig. 2 left. To obtain Theorem 1.1, the authors proved the existence of a periodic stable $\hat{p} = 3$ EPL (i.e. with residue $0 < R < 1$) and use a suitable scaling of the SM (the R_ϵ-renormalization scaling, see below) to conclude the proof. Consequently, there is a positive lower bound $K_b^{\{3\}}$ of $m_L(E_b^{\{3\}})$ such that,

$$m_L(E_b) \geq m_L(E_b^{\{3\}}) \geq K_b^{\{3\}} > 0. \tag{4}$$

However, Theorem 1.1 does not give any estimate of the value of $m_L(E_b^{\{3\}})$. In contrast, in this work we provide an analogous quantitative result. For analytical simplicity, we consider a family F_ϵ with central symmetry. Accordingly, it has no sense to consider EPL from $E_b^{\{3\}}$ because the EPL must be symmetric. Instead we consider the subset $E_b^{\{4\}} \subset E_b$ of a-parameters for which F_ϵ has a symmetric EPL of period $\hat{p} = 4$ ($p = 2$), like the one in represented in Fig. 2 right.

In Section 2 we use the SM (2) to get an accurate estimate $m_L(E_b^{\{4\}})$ for an *a priori stable* family of F_ϵ close to the integrable limit. As pointed out in [17], one expects that a similar result holds in the *a priori stable* case. Note, however, that in the *a priori unstable* case the leading approximation of the SM (2) admits a linear scaling of ϵ, the so-called R_ϵ-renormalization [8, 9, 15], used to obtain Theorem 1.1 above. In such a case one has $a = a_0(1 + o(1))$ with $a_0 = -\log(\epsilon^r/\log\lambda)/\log\lambda$ (see [15, 19]) and then, if $\epsilon_2 = \epsilon_1/\lambda^{1/r}$, it follows $a(\epsilon_2) \approx a(\epsilon_1)$ (mod 1). This scaling does not hold in the *a priori stable* context as it was observed in [8] for a concrete example and was discussed in [19] in the general setting.

We study the limit $b \to +\infty$ assuming independence between the parameters a and b in (2), as explained in Section 1.2. Then, for a fixed b, Theorem 1.1 ensures the existence of a positive lower bound for $m_L(E_b)$. To get a more quantitative result we analytically estimate $m_L(E_b^{\{4\}})$. One obtains an infinity number of a-intervals which correspond to different periods P of EPL for a generic F_ϵ. Adding them, one obtains an estimate of $m_L(E_b^{\{4\}})$. However, different EPL might coexist for some range of parameters a, that is, some a-intervals related to different EPL might overlap. We can remove the effect of the overlapping between the a-intervals corresponding to consecutive periods P, hence obtaining a much precise estimate of $m_L(E_b^{\{4\}})$. But it might happen that EPL of very different periods P give a-intervals that overlap. This effect, although expected to be almost negligible, is not considered in the theoretical results in Section 2.

Section 2.2 relates the result obtained for a fixed b with the *a priori stable* situation in which we are interested in. For an *a priori stable* family F_ϵ, with the considered properties, we denote by $E_\epsilon^{\{4\}}$ the set of parameters ϵ for which the corresponding model SM (2), with $a = a(\epsilon)$ and $b = b(\epsilon)$ according to (3), has a period $p = 2$ EPL trajectory. The union of the a-intervals of stability for different b values generates a collection of strips, below referred as EPL strips, in the (a, b)-plane (see Fig. 3 for an sketch of the situation and compare with Fig. 8 in Section 2.2 and Fig. 14 right in Section 3). We prove that the slope of the EPL strips is $\approx 1/\log(2)$ for large values of b (see Section 2.2) and, consequently, the curve $(a(\epsilon), b(\epsilon))$ (denoted by $\mathcal{C}$ in Fig. 3) corresponding to an *a priori stable* family intersects transversally these EPL strips, at least for values of $\epsilon \approx 0$ (i.e. for b large enough). This justifies our approach to get the estimate of $m_L(E_b^{\{4\}})$.

Most of the explanations in this paper are exemplified by numerical explorations. Some numerical estimates of the values of $m_L(E_b^{\{4\}})$ for values $-4 \leq -\log b \leq 4$ were also given in [17]. These

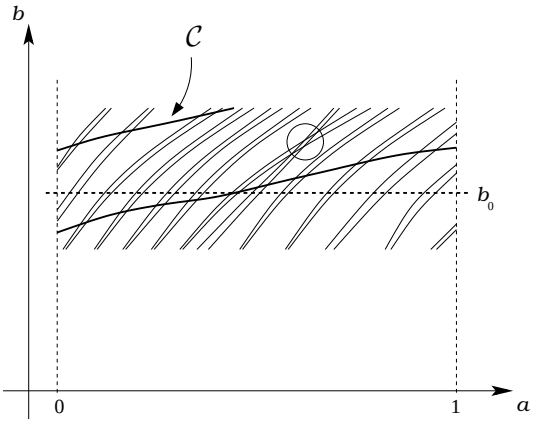

Figure 3: Sketch of the EPL strips for a range of b values large enough. Each EPL strip is related to different periodic P trajectory of F_ϵ which gives rise to a period $p = 2$ EPL. For a fixed $b = b_0$, the intersection of the EPL strips with the horizontal (dashed) line provides a collection of a-intervals of stability. An *a priori stable* family F_ϵ defines a curve $\mathcal{C}$ which intersects transversally these EPL strips. Inside the circle two EPL strips intersect and the corresponding a-intervals for these b values overlap.

computations were performed using double precision arithmetics, hence the intervals of stability of the tiny islands were not considered. On the other hand, these computations concerned the SM model (2), and no attempt was done in [17] to check the theoretical results using a family F_ϵ and relating it to the SM model. Through this work, we compare our analytical results with accurate numerical computations for *a priori stable* families F_ϵ of APMs.

In Section 2 we include a comparison between the theoretical estimates of $m_L(E_b^{\{4\}})$, for $b \to +\infty$, and the measure obtained by the direct computation of the EPL a-intervals from the SM model (2). In Section 3 we consider the standard map (from now on STM, for short)

$$\mathrm{STM}_\epsilon : \begin{pmatrix} x \\ y \end{pmatrix} \mapsto \begin{pmatrix} \bar{x} \\ \bar{y} \end{pmatrix} = \begin{pmatrix} x + \epsilon\bar{y} \\ y + \epsilon \sin(x) \end{pmatrix}, \tag{5}$$

as an example of *a priori stable* family of APMs. The parameter ϵ of the STM can be seen as a distance-to-integrable parameter. Note that it has central symmetry, hence it fits within the theoretical framework of our analytical results. Numerically, we compute the period $p = 2$ EPL inside the lobes that, for $\epsilon > 0$, the manifolds of the hyperbolic fixed point of STM create. Using a continuation procedure, we obtain an estimate of the set of ϵ parameters having EPL and compare it with the predicted theoretical results in terms of the a, b parameters of the SM model. Moreover, we describe the bifurcation pattern of these EPL.

Section 4 is devoted to illustrate EPL trajectories in an example where the related figure-eight geometry does not respect the required symmetries. We show that, although the quantitative results should be adapted, the existence of EPL and the qualitative pattern of the bifurcation curves is similar. Nevertheless, the absence of central symmetry allows for period-doubling bifurcations of EPL trajectories contrary to what happens for the SM trajectories (if considered on the figure-eight, see Lemma 3.1). Note that the proper model in this situation is a non-symmetric DSM (1). Several comments try to elucidate why we have some quantitative differences. Concretely, in Section 4 we (numerically) look for EPL inside the homoclinic lobes

of the 4-periodic islands of stability of the Hénon map family

$$H_c : \begin{pmatrix} x \\ y \end{pmatrix} \mapsto \begin{pmatrix} c(1-x^2)+2x+y \\ -x \end{pmatrix}. \tag{6}$$

The non-genericity of the $1:4$ resonance of the family (6) is reflected in the non-symmetric figure-eight that the manifolds form. In particular, for the values of interest, that is, close to the integrable limit, one of the loops is bounded by separatrices with relatively large splitting while the splitting related to the separatrices of the other loop is almost negligible (see [18] for details on these splittings). Accordingly, we look for EPL trajectories which do not visit all the homoclinic lobes but only the ones that creates the large splitting of separatrices. These EPL trajectories are of the type considered in [17], see Fig. 2 left and compare with Fig. 16 right. Despite the non-generic properties of the $1:4$ resonance for the family (6), the phenomenon we look for (existence/abundance of EPL) as well as the mechanisms of creation/destruction of EPL are expected to be generic.

This example reflects the main difficulties that appear in this type of quantitative numerical studies (some of them also appear in the STM analysis (Section 5)). We note that,

- The role of ϵ in a family F_ϵ as considered above is played in (6) by the parameter c. For $c = c_* = 1$ the $1:4$ resonant bifurcation takes place. For $c > 1$ the period-4 islands of (6) have a pendulum-like geometry and the splitting of the inner/outer separatrices have an exponentially small upper bound with respect to (some power of) $c-1$. Further details on the behavior of these splittings and several comments on the non-genericity of the $1:4$ resonance for the Hénon map can be found in [18].
- The periodic orbits inside the homoclinic lobes in a pendulum-like island, like the $1:4$ island considered for (6), must have large period T. These higher period orbits are usually stable for values of the parameter ranging on rather short intervals.
- Denote by $E(c)$ the set of c-values for which (6) has EPL visiting the homoclinic lobes related to the $1:4$ resonance. We are interested in estimates of $m_L(E(c))$ for a given c value greater than, but close to, c_*. This is equivalent to consider b large ($\epsilon \approx 0$) in the corresponding DSM model but, then, one should also take into account that changes in c cause changes in the values of both a and b in a way that depends on the distance-to-integrable parameter ϵ, see comments in Section 1.2.
- From a practical point of view it is obviously impossible to deal with all types of EPL orbits. Hence, lower bounds of $m_L(E(c))$ depend on the geometry of the EPL we look for.

To confront these difficulties and compute a lower bound of $m_L(E(c))$ in this example we proceed as follows: instead of fixing P and count the number of elliptic P-periodic orbits by scanning a homoclinic lobe, we look for EPL with some geometrical properties for "all" periods (that is, we look for elliptic P-periodic orbits with $P < P_{max}$ for a suitable maximum period P_{max}).

In Section 4 we restrict ourselves to a special type of EPL, which can be seen as a period $\hat{p} = 3$ orbits with a particular symmetry. As before, period $\hat{p}$ refers to a period related to a DSM model, hence counting an iterate each time the real dynamics of the map returns to each of the annuli that form the fundamental domain: in fact, one needs hundreds of iterates of (6) to return to the domain. As a consequence, the computations must be done using multiprecision arithmetics. On the other hand, the inherent hyperbolicity within the homoclinic lobes makes necessary to combine high precision with the use of symmetries to look for periodic orbits. This is the reason why we restrict to some specific type of EPL trajectories. In any case, a large

amount of periodic orbits is detected but the measure of the set of parameters c for which the map has stability islands related to these periodic orbits turns out to be not too large. On the other hand, we have also identified the bifurcations taking place from the creation of the stability domain until it is destroyed, for the particular orbits considered. A numerical experiment to show the stickiness properties (see [23, 24]) of the detected type of islands concludes Section 4.

Finally, Section 5 summarizes the results in this paper and opens new lines for future works.

To end this introduction we note that the numerical algorithms used through the paper are standard ones for the computation of fixed/periodic orbits and continuation with respect to parameters. Any standard book on numerical analysis can help the unfamiliarized reader. Our multi-precision algorithms, when necessary, have been coded using the Pari/GP package [21].

2 On the abundance of stability islands inside the homoclinic lobes

The dynamics within a homoclinic lobe seems to be completely chaotic and it is commonly accepted ergodicity as a reasonable assumption to describe it. However, in Section 2.1 and following [17], we show the existence of a positive measure set of parameters ϵ, below we refer them as EPL parameters, for which any close enough to integrable analytic APM F_ϵ has EPL trajectories. Concretely, we study the presence of period $p = 2$ EPL. These EPL trajectories of F_ϵ exist only for values of ϵ in an EPL strip of stability, see Fig. 3. The geometry of the EPL strips is analyzed in Section 2.2. On the other hand, in Section 2.3 we study the location of the islands related to period $p = 2$ EPL which, because the simplicity of these EPL trajectories, are expected to generate the largest stability islands in families F_ϵ with central symmetry. This might provide a preliminary insight into the density distribution law of the iterates of a map inside a homoclinic lobe, a task which is far beyond the goal of the present work.

2.1 Positive measure set of EPL parameters close to the integrable limit

Consider the two-parameter family $\mathrm{SM}_{a,b}$ given by (2). The change $\hat{x} = 1/2 - x$, $\hat{y} = y$, reverses the sign of b and hence we consider from now on $b > 0$. Recall that, although we consider the parameters a and b as independent parameters, we want to use the SM (2) to describe the dynamics of an *a priori stable* family of APMs F_ϵ. Then $\epsilon \sim b^{-1/r}$ meaning that one has to consider (2) for large values of b.

Remark. Under some reversibility conditions on the figure-eight geometry, the separatrix map $\mathrm{SM}_{a,b}$ (2) has a kind of "universal" character. In particular, the EPL pattern that we describe below might help to understand the general pattern expected for any APM for the EPL visiting homoclinic lobes created by the invariant manifolds of the hyperbolic (Birkhoff type) periodic orbits (pendulum-like resonant islands).

For a fixed b we look for the measure of the set of maps (depending on a) having EPL of period $p = 2$. This gives a collection of a-intervals for which the map $\mathrm{SM}_{a,b}$ has these trajectories. Some of the a-intervals overlap. The overlapping effect changes the estimate of $m_L(E_b^4)$ by a relatively small amount (see Theorem 2.2 and the numerical computations below).

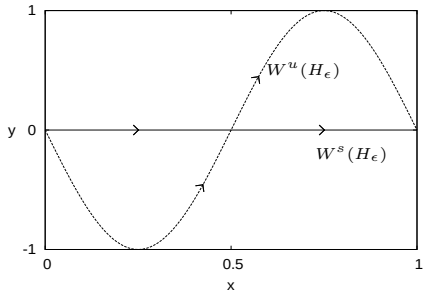

Figure 4: A sketch of the relative position of the invariant manifolds of H_ϵ in the fundamental domain $x \in [0, 1)$ where the $\mathrm{SM}_{a,b}$ (2) is defined.

Theorem 2.1 *Consider the parameter a ranging in $[0, 1)$. For a fixed b, let $\sum \Delta a$ denote the sum of the lengths of the intervals $\Delta a = (a_-, a_+)$ such that for $a \in \Delta a$ the separatrix map $SM_{a,b}$, given by (2), has an elliptic 2-periodic orbit inside the homoclinic lobe. Then,*

$$\lim_{b\to+\infty} \sum \Delta a = \frac{1}{2\pi^2} \ .$$

Proof. For simplicity, along the proof we denote by T the map $\mathrm{SM}_{a,b}$, skipping the dependence on the parameters.

The invariant manifolds of H_ϵ bound two homoclinic lobes within the domain of definition of T, see Fig. 4. We consider a point (x_0, y_0) inside the right homoclinic lobe. In particular, $x_0 > 1/2$ and $y_0 > 0$. Define $(x_k, y_k) = T^k(x_0, y_0)$ the trajectory of (x_0, y_0). Then, (x_1, y_1) must be inside the left homoclinic lobe to have a 2-periodic EPL and, in particular, $x_1 < 1/2$ and $y_1 < 0$. Hence, the condition of existence of period $p = 2$ EPL is $x_{-1} = x_1 \pmod 1$, $y_{-1} = y_1 < 0$, which gives the conditions

$$\begin{aligned} 2a + b\log(-y_0 y_1) &= 0 \pmod 1, & (7)\\ \sin(2\pi x_0) + \sin(2\pi x_1) &= 0. & (8) \end{aligned}$$

From (8) one obtain two possibilities: either $x_1 = x_0 - 1/2$ (case (i)) or $x_1 = 1 - x_0$, $x_0 \neq 3/4$ (case (ii)).

The computation of the trace of the differential matrix of T^2 at (x_0, y_0) gives

$$Tr = Trace(DT^2(x_0, y_0)) = 2 + (\beta_0 + \beta_1)(\alpha_0 + \alpha_1) + \beta_0\beta_1\alpha_0\alpha_1,$$

where $\alpha_i = 2\pi\cos(2\pi x_i)$ and $\beta_i = b/y_i$ for $i = 0, 1$. We look for elliptic-hyperbolic (E-H) bifurcations, which appear when $Tr = 2$ or $Tr = -2$. First we consider $Tr = 2$.

If we consider case (i), that is $x_1 = x_0 + 1/2$, $Tr = 2 - \alpha_0^2 b^2/y_0 y_1$. Then, in order to have an (E-H) bifurcation one should have $\alpha_0 = 0$ which implies

$$x_0 = 3/4, \ x_1 = 1/4.$$

The condition $x_1 = T_1(x_0, y_0)$ (where T_1 refers to the first component of T), gives $a + b\log(-y_1) = 1/2$, which together with condition (7) provides (recall that $\log\lambda = b^{-1}$)

$$y_0 = \lambda^k/(1 + \lambda^k), \quad \text{for some } k \in \mathbb{Z}.$$

Denote by $y_{0,k}$ the corresponding value of y_0 for a given k. Then, taking into account that $y_{1,k} = y_{0,k} - 1$, one obtains

$$a^{(\mathrm{i})}_{tr=2,k} = \frac{1}{2} - b\log(-y_1) = \frac{1}{2} + b\log(1+\lambda^k) \pmod 1.$$

Otherwise, if we consider case (ii), the condition $Tr = 2$ is given by

$$2y_0 + \sin(2\pi x_0) + \pi b\cos(2\pi x_0) = 0. \tag{9}$$

Condition (7) gives $a_{tr=2} = -b\log(-y_0 y_1)/2$. Moreover, conditions $x_1 = -x_0 \pmod 1$ and $x_1 = T_1(x_0, y_0)$ give $a_{tr=2} = -2x_0 - b\log(-y_1) \pmod 1$. Relating both expressions of a and using condition (9) one gets the equation

$$4x_0 - b\log(-\sin(2\pi x_0) - \pi b\cos(2\pi x_0)) + b\log(-\sin(2\pi x_0) + \pi b\cos(2\pi x_0)) = n,\ n\in\mathbb{Z}, \tag{10}$$

from which it can be determined $x_0 = x_{0,n}$ for each n, as we shall see. Then,

$$y_{0,n} = -\frac{1}{2}(\sin(2\pi x_{0,n}) + \pi b\cos(2\pi x_{0,n})),$$

and

$$a^{(\mathrm{ii})}_{tr=2,n} = -2x_{0,n} - b\log\left(\frac{1}{2}\left(\pi b\cos(2\pi x_{0,n}) - \sin(2\pi x_{0,n})\right)\right) \pmod 1.$$

To get an explicit (not depending on x_0) expression of $a^{(\mathrm{ii})}_{tr=2,n}$ let us consider $x_0 = 3/4 - \xi$ and look for $x_0 \in (1/2 + \arctan(\pi b)/2\pi,\ 1 - \arctan(\pi b)/2\pi)$ (for other values of $x_0 \in (1/2, 1)$ some argument of log in (10) would be negative). Expression (10) reads as

$$4\xi + b\log\left(\frac{-\pi b\cos(2\pi x_0) - \sin(2\pi x_0)}{\pi b\cos(2\pi x_0) - \sin(2\pi x_0)}\right) = k, \qquad k = 3 - n,$$

or, equivalently,

$$\frac{1+\pi bt}{1-\pi bt} = \lambda^{k-4\xi},$$

where $t = \tan(2\pi\xi) = \cos(2\pi x_0)/\sin(2\pi x_0)$ and, hence, $t \in (-1/\pi b, 1/\pi b)\setminus\{0\}$. It is clear that for each $k\in\mathbb{Z}$ this equation has a unique solution: the left hand side increases from 0 to ∞ and the right hand side is positive and decreasing. Last equation can also be written as a fixed point equation

$$\xi = \frac{1}{2\pi}\arctan\left(\frac{\lambda^{k-4\xi} - 1}{\pi b(\lambda^{k-4\xi}+1)}\right). \tag{11}$$

Note that the replacement of k by $-k$ changes the solution from ξ to $-\xi$. Furthermore, equation (11) defines a contraction if $b > 1/\pi$.

Then, for a given k one determines $\xi = \xi_k$ and, by substituting in the expression of $a^{(\mathrm{ii})}_{tr=2,n}$, it is found

$$a^{(\mathrm{ii})}_{tr=2,k} = \frac{1}{2} - 2\xi_k - b\log c_k + b\log(1+\lambda^{4\xi_k - k}),\ (\mathrm{mod}\ 1), \qquad k\in\mathbb{Z},$$

where we have introduced the notation $c_k = \cos(2\pi\xi_k)$.

We consider now $Tr = -2$. We recall that in case (i) one has $Tr = 2 - (\alpha_0^2 b^2/y_0 y_1) \geq 2$. On the other hand, if we look for (E-H) bifurcations that appear when $Tr = -2$ (case (ii)) the analogous of equation (9) reads

$$y_0^2 + (\sin(2\pi x_0) + 2\pi b\cos(2\pi x_0))y_0 + \pi b\cos(2\pi x_0)(\sin(2\pi x_0) + \pi b\cos(2\pi x_0)) = 0$$

which gives either $y_0 = -\pi b \cos(2\pi x_0)$ (we refer below by (ii.1) to this case) or $y_0 = -\sin(2\pi x_0) - \pi b \cos(2\pi x_0)$ (below referred by (ii.2)). The conditions $y_0 > 0, y_1 < 0$ restrict the validity of the solution (ii.1) to the range $1/2 + \arctan(\pi b)/2\pi < x_0 < 3/4$, and the validity of (ii.2) to the range $3/4 < x_0 < 1 - \arctan(\pi b)/2\pi$. Then, if we consider (ii.1) the analogous of equation (10) reads

$$4x_0 - b\log(-\pi b\cos(2\pi x_0)) + b\log(\pi b\cos(2\pi x_0) - \sin(2\pi x_0)) = n,\ n \in \mathbb{Z}, \tag{12}$$

while, considering (ii.2), one obtains

$$4x_0 + b\log(\pi b\cos(2\pi x_0)) - b\log(-\pi b\cos(2\pi x_0) - \sin(2\pi x_0)) = n,\ n \in \mathbb{Z}. \tag{13}$$

For each n, after determining $x_0 = x_{0,n}$ from (12), one has $y_{0,n} = -\pi b\cos(2\pi x_{0,n})$ and

$$a^{(\text{ii.1})}_{tr=-2,n} = -2x_{0,n} - b\log(\pi b\cos(2\pi x_{0,n}) - \sin(2\pi x_{0,n})) \pmod 1.$$

Analogously, after determining $x_{0,n}$ from (13), then $y_{0,n} = -\sin(2\pi x_{0,n}) - \pi b\cos(2\pi x_{0,n})$ and

$$a^{(\text{ii.2})}_{tr=-2,n} = -2x_{0,n} - b\log(\pi b\cos(2\pi x_{0,n})) \pmod 1.$$

As before, by considering $x_0 = 3/4 - \eta$, $t = \tan(2\pi\eta)$, from equation (12) one obtains the equation

$$\frac{\pi b t}{1 - \pi b t} = \lambda^{k-4\eta}$$

or, in the form of fixed point equation

$$\eta = \frac{1}{2\pi}\arctan\left(\frac{\lambda^{k-4\eta}}{\pi b(\lambda^{k-4\eta}+1)}\right), \quad k \in \mathbb{Z}, \tag{14}$$

while, from equation (13), one obtains

$$-\frac{1 + \pi b t}{\pi b t} = \lambda^{k-4\eta}$$

or, in the form of fixed point equation

$$\eta = \frac{1}{2\pi}\arctan\left(\frac{-1}{\pi b(\lambda^{k-4\eta}+1)}\right), \quad k \in \mathbb{Z}. \tag{15}$$

One easily checks that these equations have a unique solution for any $k \in \mathbb{Z}$ and that replacing k by $-k$ changes the solution from η to $-\eta$. Equations (14) and (15) define contractions for $b > 1/(\sqrt{2}\pi)$.

In both cases, for a given k one obtains $\eta = \eta_k$ and it turns out that $a^{(\text{ii.1})}_{tr=-2,k} = a^{(\text{ii.2})}_{tr=-2,k}$ and, hence, it will be denoted below as $a^{(\text{ii})}_{tr=-2,k}$. Let $c_k = \cos(2\pi\eta_k)$, then

$$a^{(\text{ii})}_{tr=-2,k} = \frac{1}{2} + 2\eta - b\log c_k + b\log(1 + \lambda^{k-4\eta}) \pmod 1.$$

The Fig. 5 shows the behavior of x_0 for different values of n considered as a continuous parameter (recall that $k = 3 - n$) according to the different cases explained above. The figure has been computed for $b = 1$ to make easy to understand the plot. For larger b, the three curved lines represented are closer to the vertical line making not so easy to differentiate the regions. For smaller b the range of x_0 is wider, but the curves have smaller slope at $n = 3$ and tend quickly to the limit when n increases or decreases. However, the qualitative picture remains invariant for all b values.

The following facts can be easily checked from the above expressions (compare with Fig. 5).

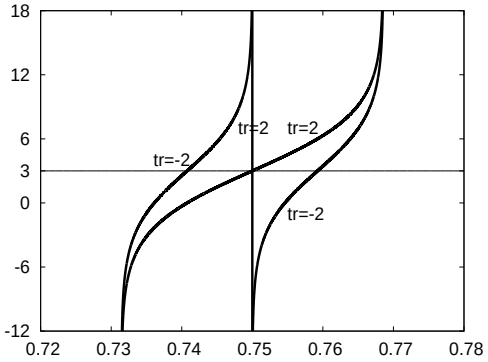

Figure 5: Behavior of the solutions x_0 of equations (10) and (12) corresponding to case (ii) (curved lines) and to the case (i) (vertical line through $x_0 = 0.75$). In the vertical axis we represent the value of n and the values of the solutions x_0 range the horizontal axis. The line $n = 3$ is shown to emphasize the symmetries of the figure (see text for details).

1. x_0 is a solution of the equation (10) for a fixed n if, and only if, $\hat{x} = 3/2 - x_0$ is a solution of (10) with $\hat{n} = 6 - n$.
2. x_0 is a solution of equation (12) for a fixed n if, and only if, $\hat{x} = 3/2 - x_0$ is a solution of equation (13) with $\hat{n} = 6 - n$.
3. $a^{(\mathrm{i})}_{tr=2,k} = a^{(\mathrm{i})}_{tr=2,-k}$, $a^{(\mathrm{ii})}_{tr=2,k} = a^{(\mathrm{ii})}_{tr=2,-k}$, and $a^{(\mathrm{ii})}_{tr=-2,k} = a^{(\mathrm{ii})}_{tr=-2,-k}$, where all the values of a considered should be taken modulus 1.

In particular, we add below the lengths of the a-intervals with 2-periodic EPL such that $x_0 < 3/4$ (the others with $x_0 > 3/4$ give the same a-intervals and, therefore, are not considered in the sum of the lengths). Hence, in the Table 1 we sum up, according to the value of k, the end points of the a-intervals of 2-periodic EPL with $x_0 < 3/4$ (hence with $\xi, \eta > 0$) that we should consider.

	$a_{tr=2}$	$a_{tr=-2}$
$k > 0$	$1/2 - 2\xi_k - b\log c_k + b\log(1+\lambda^{4\xi_k - k})$	$1/2 - 2\eta_k - b\log c_k + b\log(1+\lambda^{4\eta_k - k})$
$k < 0$	$1/2 + b\log(1+\lambda^{k})$	$1/2 + 2\eta_k - b\log c_k + b\log(1+\lambda^{k-4\eta_k})$

Table 1: Different values of a corresponding to extremes of intervals for which there is a 2-periodic EPL with $x_0 < 3/4$. In the first column c_k denotes $\cos(2\pi\xi_k)$, while in the second one denotes $\cos(2\pi\eta_k)$. The value of ξ_k is obtained as solution to the equation (11) while the values η_k are solutions of (14).

We are interested on the length Δa of the intervals having endpoints $a_{tr=2}$ and $a_{tr=-2}$. Furthermore we recall that we want to see the behavior for large b and that just $b > 1/\pi$ is enough to ensure that the fixed point equations for ξ, η are contractions. To see how the widths behave for different values of k we introduce $\alpha = k/b$. Then $\exp(\alpha) = \lambda^k$, and we distinguish the cases $\alpha \leq 0$ and $\alpha > 0$. For simplicity, we do not write the dependence on k in what follows, despite it should be kept in mind.

For $\alpha \leq 0$, as equation (14) defines a contraction for b large enough, the following fixed point is obtained by iteration

$$\eta = \frac{e^{\alpha}}{2\pi^2 b(1+e^{\alpha})} + \mathcal{O}(b^{-2}),$$

which allows to compute

$$a^{(i)}_{tr=-2} = \frac{1}{2} + b\log(1+\lambda^k) + \frac{1}{\pi^2 b}\left(\frac{m}{1+m} - \frac{3}{2}\left(\frac{m}{1+m}\right)^2\right) + \mathcal{O}(b^{-2}),$$

where m denotes e^{α} and hence

$$\Delta a = \frac{1}{\pi^2 b}\left(\frac{m}{1+m} - \frac{3}{2}\frac{m^2}{(1+m)^2}\right) + \mathcal{O}(b^{-2}), \quad \alpha \leq 0. \tag{16}$$

For $\alpha > 0$ we proceed in a similar way solving by iteration equations (11) and (14). It is convenient to write the solutions as

$$\xi = \frac{1}{2\pi^2 b}\frac{1-e^{-\alpha}}{1+e^{-\alpha}} + \mathcal{O}(b^{-2}), \qquad \eta = \frac{1}{2\pi^2 b}\frac{1}{1+e^{-\alpha}} + \mathcal{O}(b^{-2}),$$

which allows to compute

$$a^{(ii)}_{tr=2} = \frac{1}{2} + b\log(1+\lambda^k) - \frac{1}{\pi^2 b}\frac{1-m}{1+m} + \frac{1}{2\pi^2 b}\frac{(1-m)^2}{(1+m)^2} + \frac{2}{\pi^2 b}\frac{m(1-m)}{(1+m)^2} + \mathcal{O}(b^{-2}),$$

$$a^{(ii)}_{tr=-2} = \frac{1}{2} + b\log(1+\lambda^k) - \frac{1}{\pi^2 b}\frac{1}{1+m} + \frac{1}{2\pi^2 b}\frac{1}{(1+m)^2} + \frac{2}{\pi^2 b}\frac{m}{(1+m)^2} + \mathcal{O}(b^{-2}),$$

where now m denotes $e^{-\alpha}$ and hence

$$\Delta a = \frac{1}{2\pi^2 b}\frac{m^2}{(1+m)^2} + \mathcal{O}(b^{-2}), \quad \alpha > 0. \tag{17}$$

In particular, one gets for the total sum of the lengths of the a-intervals for $\alpha \leq 0$ and $\alpha \geq 0$ by approximating the sums by integrals. Putting both contributions together we have

$$\sum \Delta a = \int_0^1 \frac{1}{\pi^2}\left(\frac{m}{1+m} - \frac{3}{2}\frac{m^2}{(1+m)^2} + \frac{1}{2}\frac{m^2}{(1+m)^2}\right)\frac{dm}{m} + \mathcal{O}\left(\frac{1}{b}\right) = \frac{1}{\pi^2}\int_0^1 \frac{1}{(1+m)^2}dm + \mathcal{O}\left(\frac{1}{b}\right) =$$

$$\frac{1}{2\pi^2} + \mathcal{O}\left(\frac{1}{b}\right). \qquad \square$$

Remark. From expression (16) one obtains that the maximum width of the intervals with $\alpha \leq 0$ is obtained for $m = 1/2 + \mathcal{O}(1/b)$, that is, for $\alpha = -\log(2) + \mathcal{O}(1/b)$. In contrast, from expression (17), one easily checks that Δa is a monotonically decreasing function with respect to α for $\alpha > 0$.

Note that to get the value of Theorem 2.1 we add the length of all the a-intervals. However, some of them overlap, a fact which in the result above is not considered. Some comments might help to clarify this point. For a fixed b, let us consider, for positive k, the values of $a^{(i)}_{tr=2,-k}, a^{(i)}_{tr=-2,-k}, a^{(ii)}_{tr=2,k}, a^{(ii)}_{tr=-2,k}$ that we denote, for shortness, a^1, a^2, a^3, a^4, respectively. From the expressions given above it is immediate to check that, for k small, one has $a^3 < a^1 < a^4 < a^2$ and, hence, there is an overlap whose length amounts to $a^4 - a^1$. This happens until $k \approx b\log(2)$, while for larger values of k one has $a^3 < a^4 < a^1 < a^2$ and no overlap occurs. The size of the overlap for a given k is $\frac{1}{2\pi^2 b}\frac{2m-1}{(1+m)^2}$ and the sum of the overlaps from $k = 1$ to $k = b\log(2)$ is

$$\text{overlap} = \frac{1}{2\pi^2}\int_{1/2}^1 \frac{2m-1}{(1+m)^2}\frac{dm}{m} = \frac{1}{2\pi^2}(1/2 - \log(3/2)).$$

Summarizing we have proved

Theorem 2.2 *The sum of the lengths of the intervals in a for which the separatrix map $SM_{a,b}$, given by (2), has an elliptic 2-periodic orbit inside the homoclinic lobe, skipping the elementary overlaps which occur for $\pm k \in (0, b\log(2))$ tends, when $b \to \infty$ to*

$$\frac{1}{2\pi^2}(1/2 + \log(3/2)). \qquad \square$$

Note that the value given by Theorem 2.1 is ≈ 0.0506605918, while the value given by Theorem 2.2 is ≈ 0.0458713982. However, one observes also overlapping between a-intervals obtained for values of $k < -b\log(2)$ (resp. $k > b\log(2)$) in the $\alpha < 0$ (resp. $\alpha > 0$) case. See comments in Section 2.2 and Fig. 8 center. This phenomenon is not taken into account in Theorem 2.2, but we believe that its effect on the total measure of the EPL parameters, at least for b large enough, is not very relevant. As an example we have computed for $b = 5000$ and k ranging from -66667 to 33333 the sum of the lengths of the a intervals with EPL orbits. The result is $\sum \Delta a = 0.0506603862$, quite close to the value given in Theorem 2.1. Then we have skipped all the lengths corresponding to overlaps. The number of non-overlapped intervals reduces from 100001 to 92265, and the sum of its lengths is 0.0448529310, quite close to the value obtained in Theorem 2.2. Note that the number of overlapped intervals discarded in Theorem 2.2 is $5000 \times \log(2) \approx 3465$. Hence the number of additional overlaps discarded is 4271, but they are extremely small.

Numerically it is possible to scan the intervals above for many values of b (by means of a continuation method we look for values of a with $Tr = 2$ and $Tr = -2$). Let μ such that $\lambda = \exp(\exp(\mu))$. Then $b = 1/\log(\lambda) = \exp(-\mu)$ and, hence, the integrable limit is obtained for $\mu \to -\infty$. The Fig. 6 left shows the value of the sum of the intervals as a function of μ. According to Theorem 2.1 it converges to the value $1/(2\pi^2) \approx 0.0506605918$. The right plot shows the behavior of the sum of the lengths of the intervals removing the overlapping. Note that, after removing the overlapping, the sum of the lengths converges to some positive constant $K \approx 0.0444$, obtaining an analogous result to the one in [17] but in a more quantitative way.

The numerical value of K obtained, $K \approx 0.0444$ according to Fig. 6 right, is slightly below the predicted above in Theorem 2.2. As said, last result does not take into account the overlapping between a-intervals obtained for different k values. On the other hand, there is the natural limitation of the numerical scanning process to detect EPL inside the homoclinic lobe: EPL with very small size of stability domain surrounded them (below some threshold related to the tolerance of the scanning process and the step in a considered for a fixed b) are not detected and the (also small) a-intervals are not considered.

Remark. Different islands of stability related to $p = 2$ EPL trajectories were illustrated in [17], see also Fig. 10 below.

As an additional information, we proceed in the same numerical way as before but performing the continuation to get period $p = 3$ EPL instead. These EPL trajectories have $\hat{p} = 6$ on the figure-eight representation and they visit both families of homoclinic lobes, see Fig.7. The results are summarized in Table 2. One checks that the contribution of the orbits with $p = 3$ is small compared to the one of the orbits with $p = 2$.

2.2 Evolution of the a-intervals with respect to b

As detailed in Section 1.2, for an *a priori stable* family of APMs both parameters a and b of the SM model (2) change as the distance-to-integrable parameter ϵ evolves. The concrete one

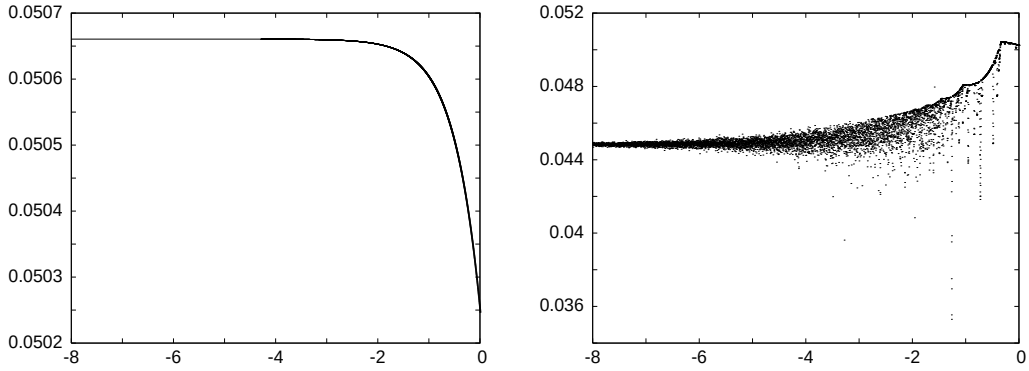

Figure 6: On the left it is shown the sum of the lengths of the intervals as a function of $\mu = -\log b$. The right part shows the same but taking into account that some intervals overlap. In both cases the measure converges to a positive constant.

μ	# intervals (1)	Sum of the lengths (2)
-1	14382	0.80968857E-02
-2	188626	0.28463994E-02
-3	339292	0.98175729E-03

Table 2: Compendium of results numerically obtained for 3-periodic orbits.
(1) Some of the stability intervals correspond to the same $p = 3$ EPL.
(2) The length has been computed removing overlapping of the intervals.

parameter family F_ϵ under consideration defines, as ϵ varies, a curve $\mathcal{C}$ in the (a, b)-parameter space, see Fig. 3 (also Fig. 14 right). In this section, we want to describe how evolves, as a function of b, the location of the a-intervals of EPL parameters.

In Fig. 8 we represent the a-intervals (as described in Theorem 2.1) for $100 < b < 101$ and $|k| < 100$. We observe a complicate structure of "main" curves, going from $b = 100$ to $b = 101$, all of them with a similar slope. Each "main" curve corresponds to a different k value. In the center plot we show the corresponding "main" curves for $k = 75$ and $k = 88$.

Each "main" curve observed in the left (and center) plots actually correspond to four curves (see Fig. 8 right). These four curves are obtained by joining the extrema of the a-intervals for different b values and, hence, define two EPL strips of stability: parameters inside these EPL strips correspond to period $p = 2$ EPL parameters. We note that some of these strips intersect other strips for a range of b values. For these b values, the corresponding a-intervals overlap.

From the expressions $a = a(b)$ in Table 1 it is immediate to check that the slope of the strips of stability in Fig. 8 is $db(a)/da = 1/\log(2) + \mathcal{O}(1/b)$. On the other hand, we concluded in Section 1.2 that the slope of the curve $\mathcal{C}$ that describes an *a priori stable* family of APMs is such that $\lim_{\epsilon\to 0} db(\epsilon)/da(\epsilon) = 0$. In particular, since $\epsilon \to 0$ corresponds to $b \to \infty$, the strips of stability must be transversal at least for values of ϵ small enough. In other words, the curve $\mathcal{C}$ crosses all the strips of stability obtained for all values of k. This simple transversality argument justifies our approach in Section 2.1 to study the set of (a, b) parameters with EPL. To illustrate this transversality property in Section 3 we approximate the curve $\mathcal{C}$ for the STM family (Fig. 14 right).

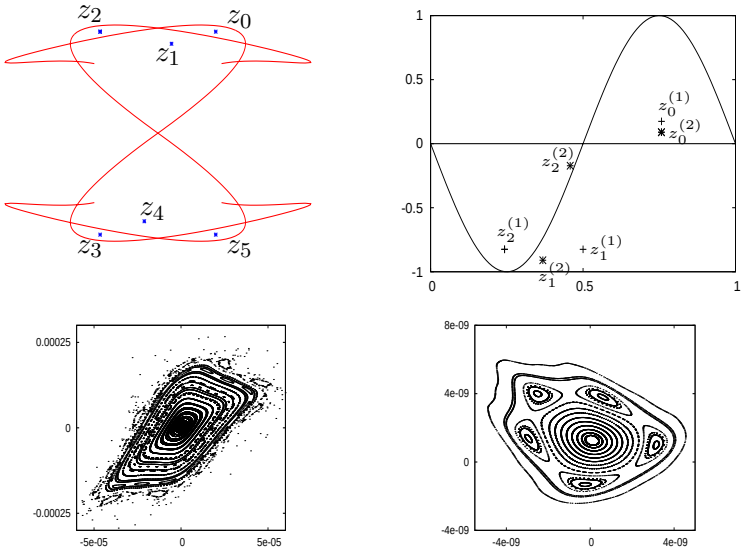

Figure 7: Top left: Schematic representation of a $p = 3$ EPL trajectory on the figure-eight. One has $z_{i+3} = Z_\epsilon(z_i)$, $i = 1, 2, 3$. Top right: Iterates of two $p = 3$ EPL for $\mu = -1$. The trajectory $\{z_0^{(1)}, z_1^{(1)}, z_2^{(1)}\}$ corresponds to $a = 0.266212$, while the trajectory $\{z_0^{(2)}, z_1^{(2)}, z_2^{(2)}\}$ corresponds to $a = 0.86798217164664582$. Bottom left: Island of stability around $z_1^{(1)} \approx (0.50000098, -0.82479289)$. Bottom right: Island of stability around the iterate $z_2^{(2)} \approx (0.45786551, -0.17242661)$. In the bottom plots we use translated coordinates to have the islands centered at the origin and better observe their size.

2.3 On the location of the 2-periodic EPL inside a homoclinic lobe

Let us comment on the position of the EPL discussed in Theorem (2.1) inside the homoclinic lobe. In Fig. 9 (left and center plots) we sketch the relative position, in the phase space, inside the right homoclinic lobe of Fig. 4, of the points $(x_{0,k}, y_{0,k})$ corresponding either to a $Tr = 2$ or $Tr = -2$. We have chosen $b = 10$ for the illustration because for larger values of b the lines are closer to the vertical line $x = 3/4$ and it is more difficult to appreciate the details. We observe that the 2-periodic EPL of Theorem (2.1) are located close to $x = 3/4$. The center plot of Fig. 9 is a magnification of the left one. The EPL islands of stability are created (by means of a saddle-center bifurcation except for $k = 0$ where a degenerated saddle-center bifurcation occurs, see below), for the suitable a value, at the points on the lines labelled by tr $= 2$. These two lines cross in the corresponding solution obtained for $k = 0$ ($n = 3$). Increasing a they move (almost) horizontally towards the closest line labelled with tr $= -2$ where the EPL are destroyed (by means of a period-doubling bifurcation).

As k increases (or $n = 3 - k$ decreases) the points $(x_{0,k}, y_{0,k})$ in Fig. 9 (center) move towards the sinusoidal curve that delimits the homoclinic lobe. For $n = 3$, both EPL trajectories are born at $(x_{0,0}, y_{0,0}) = (3/4, 1/2)$, for the same value of a. Let us analyze the phase space structure obtained for the degenerate case $n = 3$ (see simulations of the separatrix map shown in [17] for $a > a_{tr=2}$, $b = \exp(-4)$ and $n = 3$). The Fig. 9 right shows a sketch of the phase space at the bifurcation taking place for $n = 3$. The main feature of this configuration is the existence of 4 fixed points (2 elliptic and 2 hyperbolic points) bifurcating at the same time.

The degenerated saddle-center bifurcation shown in Fig. 9 right takes place, for the separatrix

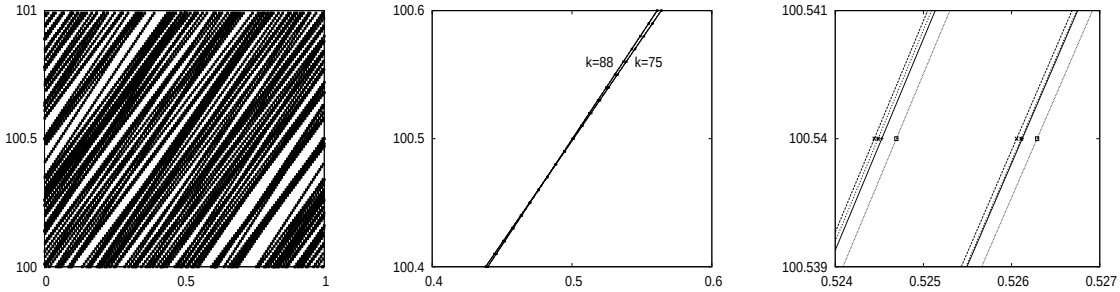

Figure 8: Parameter space (a, b) of the $\mathrm{SM}_{a,b}$ (2). Left: we represent the a-intervals for $|k| < 100$ and $100 < b < 101$. Different "main" curves, from $b = 100$ to $b = 101$, are observed. Center: Detail of intersection between the $k = 75$ and the $k = 88$ "main" curves. Right: We magnify the two "main" curves of the center plot for $b = 100.54$. Each "main" curve is formed by four lines. For each group of four lines (which correspond to the same k) the a values, from left to right, correspond to $tr = -2$, $tr = 2$, $tr = -2$ and $tr = 2$, respectively. These lines define, hence, two strips of stability where period $p = 2$ EPL exist.

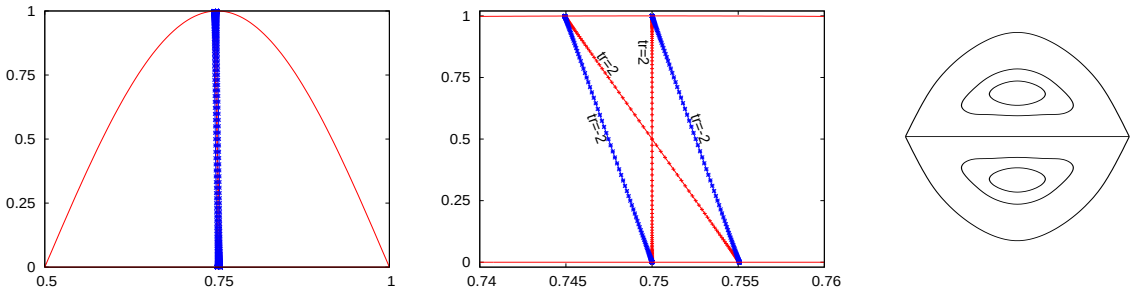

Figure 9: Left: Location, inside the homoclinic lobe, of the points where takes place either a period doubling or a saddle-center bifurcation for some a value ($b = 10$). Center: Magnification of the left plot where the corresponding curves are observed. Period $p = 2$ EPL trajectories, if exist, are located, roughly, inside the two triangular regions delimited by these curves. Right: Sketch of the degenerate structure of the saddle-node bifurcation which occurs for $n = 3$.

map, for all b values. To check the last assertion, since the bifurcation takes place at the point $(x, y) = (3/4, 1/2)$ at value $a = a_{tr=2}$, we introduce new coordinates $(x_{\mathrm{new}}, y_{\mathrm{new}}) = (x - 3/4, y - 1/2)$ to translate it to the origin and a new parameter $\epsilon = 2a - 2b\log(2) + 1$. In the following we denote again by (x, y) the new coordinates $(x_{\mathrm{new}}, y_{\mathrm{new}})$, and we denote by T the SM (2) expressed in the new coordinates. A direct computation gives $T^2(x, y) = (\bar{x}, \bar{y})$ being

$$\begin{pmatrix} \bar{x} \\ \bar{y} \end{pmatrix} = \begin{pmatrix} x + \epsilon + 2b\log 2 - 1 + b\log|y + \sin(2\pi\hat{x}) + 1/2| + b\log|\bar{y} + 1/2| \pmod 1 \\ y + \sin(2\pi\hat{x}) + \sin\left[2\pi\left(\hat{x} + \epsilon/2 + b\log 2 - 1/2 + \log|y + \sin(2\pi\hat{x} + 1/2)|\right)\right] \end{pmatrix},$$

where $\hat{x} = x + 3/4$. Expanding last expression in powers of x, y and ϵ, and looking for solutions $x = y = \mathcal{O}(\sqrt{\epsilon})$, one obtains

$$\begin{aligned} \bar{x} &= x + \epsilon - 4b\pi^2x^2 - 4by^2 - 16b^3\pi^2y^2 + 16b\pi^2xy + \mathcal{O}(\epsilon\sqrt{\epsilon}) \pmod 1 \\ \bar{y} &= y - 8\pi^2b^2y^2 + 8\pi^2bxy + \mathcal{O}(\epsilon\sqrt{\epsilon}). \end{aligned}$$

From last expression one can relate the map T^2 with a Hamiltonian flow $\varphi^{\mathcal{H}}$, that is, $T^2(x, y) \approx$

$\varphi^{\mathcal{H}}_{t=1}(x,y)$ with

$$\mathcal{H}(x,y) = 4b\pi^2x^2y + \frac{4}{3}by^3 + \frac{16}{3}b^3\pi^2y^3 - 8b^2\pi^2xy^2 - \epsilon y + \mathcal{O}(\epsilon^2)$$

The vector field $\dot{x} = -\partial\mathcal{H}/\partial y$, $\dot{y} = \partial\mathcal{H}/\partial x$ has 4 fixed points. Ignoring the effect of the $\mathcal{O}(\epsilon\sqrt{\epsilon})$ terms (which can be taken into account at the end by using the implicit function theorem), two of the fixed points are located on $y = 0$ and $x = \pm\sqrt{\epsilon}/(2\pi\sqrt{b})$, while the other two fixed points are located on $y = x/b$ and have $x = \sqrt{\epsilon b}/(2\sqrt{1+b^2\pi^2})$. The two pairs of fixed points collide for $\epsilon = 0$ (i.e. for $a = a_{tr=2} = b\log 2 + 1/2 \pmod 1$). Moreover, one easily checks that the points on $y = 0$ are hyperbolic while the points on $y = x/b$ are elliptic. The hyperbolic fixed points have energy $\mathcal{H} = 0$, while the elliptic points have the energy values $\mathcal{H} = \mp\epsilon\sqrt{\epsilon}/(3b(1+b^2\pi^2))$, respectively.

In Fig. 10 we illustrate the corresponding phase space of T^2, for $b = 1$, $\epsilon > 0$. As can be observed, the 4 fixed points of T^2 are approximately located on $y = 0$ and on the line $y = x$.

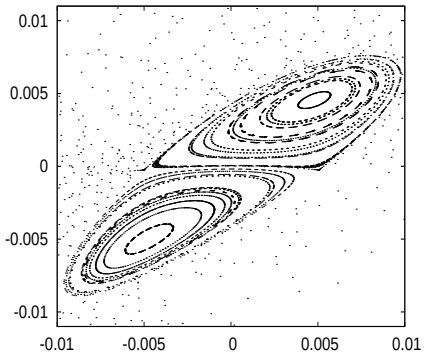

Figure 10: The degenerated saddle-center bifurcation taking place for $n = 3$. The iterates correspond to the map T^2 with $b = 1$ and $\epsilon = 10^{-3}$.

Remark. The dynamics on the separatrix $y = 0$ of Hamiltonian flow related to $\mathcal{H}$ is given by $\dot{x} = \epsilon - 4b\pi^2x^2$. The dominant singularity is located at $t = i/\sqrt{16b\epsilon}$ and the positive eigenvalue of the hyperbolic point is $\nu = 4\pi\sqrt{b\epsilon}$. Hence the splitting σ of the separatrices that separate the two islands of stability is expected to behave exponentially small with respect to ϵ, that is, $\sigma \sim \exp(-C/\epsilon)$, A, B arbitrary constants and $C = -\pi/(8b)$. This implies, see [15, 19], that for larger values of b the size of the islands of stability, as a function of ϵ, decreases faster (i.e. the related a-interval of stability is shorter). Also the splitting of the other two separatrices plays a role in the destruction of the rotational curves forming the tiny islands of stability. They role can be examined applying the techniques in [19] to the above Hamiltonian $\mathcal{H}$ in order to measure the size of the chaotic zone surrounding the separatrices.

3 Period $p = 2$ EPL for the standard map

As a first example we consider the well-known standard map STM_ϵ given by (5). We look for ϵ-intervals for which the map (5) has EPL. Concretely, we scan for period $\hat{p} = 4$ EPL inside the homoclinic lobe with label 1 in Fig. 11. After a suitable number of iterates of STM_ϵ, the trajectory visits the lobe 2. Then, after some more iterates, it moves to the lobe 3 and after to the lobe 4. Finally, it comes back to the initial point in lobe 1. Equivalently, this trajectory has

period $p = 2$: the SM trajectory jumps from 1 to 4 (Z_ϵ identifies a point in 2 with a point in 4) and comes back to 1. These are orbits like the ones considered in the previous section.

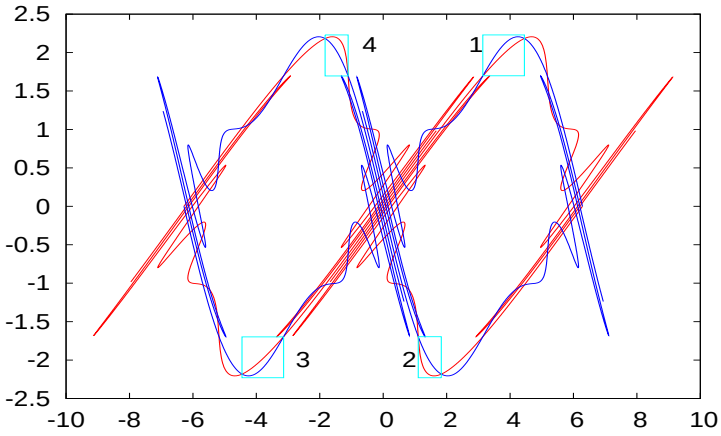

Figure 11: We represent the separatrices related to the hyperbolic point $(0, 0)$ of the map (5) for $\epsilon = 1.2$. A period $p = 2$ EPL starting inside the homoclinic lobe labelled with 1. follows a trajectory such that, after a suitable number of iterates of STM_ϵ, moves to the lobe 2. Then, performing more iterates of the map, the trajectory moves to 3. and after to 4. Finally, it comes back to the initial point in 1.

The STM admits the central involution $S : (x, y) \mapsto (-x, -y)$ (that is, $F^{-n}(x, y) = (S \circ F^n \circ S)(x, y)$). This implies central symmetry on the figure-eight, hence STM_ϵ fits within our analytical framework of Section 2. On the other hand, the presence of this symmetry simplifies our numerical computations: if we denote by (x_i, y_i) the point of the EPL trajectory inside the lobe i according to Fig. 11, then it is enough to require that $(x_3, y_3) = -(x_1, y_1)$ to have a period $p = 2$ EPL. If, moreover, $(x_3, y_3) = F^k(x_1, y_1)$ then the EPL has period $P = 2k$.

To look for such a type of EPL we perform an scanning process. Typically, for a fixed ϵ, one finds several periodic orbits (x_1, y_1) of different even periods $P = 2k$ but most of them are hyperbolic. To get EPL trajectories, we continue these (hyperbolic) periodic orbits with respect to the parameter ϵ until we get an elliptic orbit, that is, if A denotes the differential of STM_ϵ at the point (x_1, y_1) we require $|Tr(A)| < 2$.

We illustrate in Fig. 12 the pattern observed for the curves in the $(\epsilon - Tr)$-plane obtained by continuation of periodic orbits (below p.o. for short) of the type considered. The most observed pattern is similar to the one shown in Fig. 12 left, hence defining two ϵ-intervals of stability. The p.o. goes through a saddle-center bifurcation for $\epsilon \approx 0.741541270175$ while for $\epsilon \approx 0.7412179615259$, $\epsilon \approx 0.741097371094$ and $\epsilon \approx 0.741202305095$ it goes through a pitchfork bifurcation (either supercritical or subcritical). We observe also that the curve touches twice the horizontal line $Tr = -2$. However, there is not a bifurcation taking place at the corresponding values of ϵ. This pattern has been observed for most of the $p = 2$ EPL (naturally, the bifurcations take place for different values of ϵ).

For some p.o., a few of them, we observe a pattern like the one shown in Fig. 12 right. The bifurcations taking place are the same as in the left figure. The p.o. undergoes a pitchfork bifurcation (either supercritical or subcritical) for $\epsilon \approx 0.816134986710$, $\epsilon \approx 0.816094714110$ and $\epsilon \approx 0.81575456061$ while it goes through a saddle-center bifurcation for $\epsilon \approx 0.815753455388$. The two small figures are magnifications of the large right one to show concrete details of the

$\epsilon - Tr$ curve. Note that this curve provides only one ϵ-interval of stability for which exists an EPL.

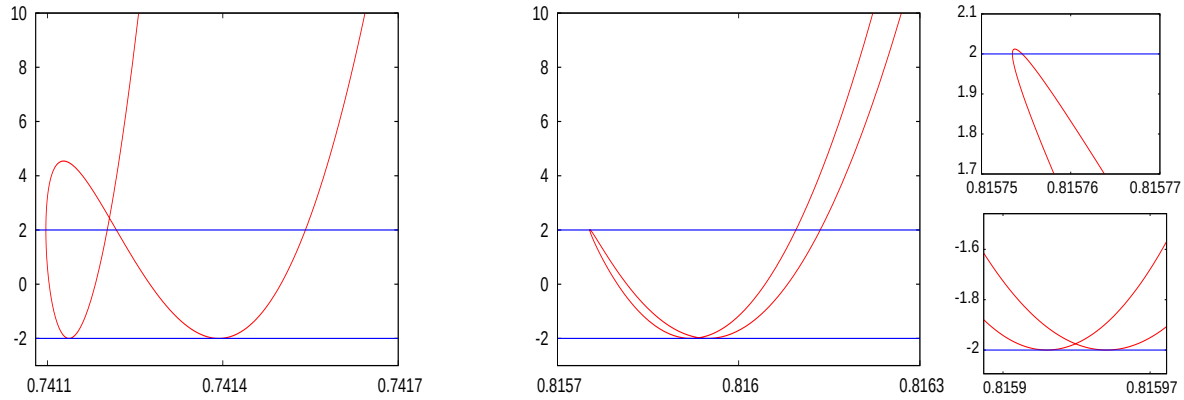

Figure 12: Two different patterns observed in the continuation of a p.o. of the type considered: in the x-axis we represent ϵ while in the y-axis the trace of the differential matrix of the STM (5) at the p.o. In the left situation we obtain two ϵ-intervals of EPL parameters, while in the right one only one. The two small plots are magnifications of the right curve.

We want to explain why the patterns shown in Fig. 12 are the expected ones according to our theoretical considerations on the SM model (2). In Section 2.1, we related a pair of a-intervals of stability to a given $p = 2$ EPL. It can happen that the EPL trajectory becomes hyperbolic because it crosses the value $a = a_{tr=2}$ and it undergoes a pitchfork bifurcation, or because it crosses the value $a = a_{tr=-2}$ and the trajectory suffers a period-doubling bifurcation. On the other hand, an STM trajectory has its equivalent trajectory on a figure-eight (see Section 1.3). In order to explain why the EPL trajectories for the STM do not suffer a period-doubling bifurcation (i.e. the curves in Fig. 12 never cross the line $Tr = -2$) let us relate the SM trajectories with the corresponding trajectories on the figure-eight.

Assume that a $p = 2$ EPL trajectory has suffered either a pitchfork or a period-doubling bifurcation. Then, generically, the invariant manifolds of the $p = 2$ p.o. (which after the bifurcation is hyperbolic) form a figure-eight inside the homoclinic lobe. We schematically represent the geometrical situation in Fig. 3. The iterates of the $p = 2$ EPL visit the lobes $1, 2, 3$ and 4 successively. We denote an iterate of a trajectory on the figure-eight by the number of the lobe where it is located and the subindex l (resp. r) if it is located inside the left loop (resp. the right loop) of the smaller figure-eight inside the lobe, according to Fig. 3. Let $\widehat{SM}$ denote the symmetric DSM map defined on the figure-eight.

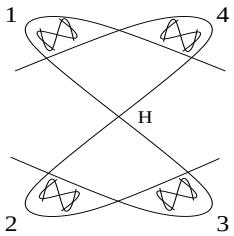

Figure 13: Sketch of the geometry after either a period-doubling or a pitchfork bifurcation of a $p = 2$ EPL.

Lemma 3.1 *Assume that the map $\widehat{SM}$ commutes with the central symmetry Z with respect to the hyperbolic point H. Then, a period $\hat{p} = 4$ EPL on a figure-eight cannot suffer a period-doubling bifurcation.*

Proof. Consider the figure-eight inside the homoclinic lobe 1 and assume that the EPL trajectory inside the left loop of this figure-eight corresponds to a $\hat{p} = 8$ EPL. We denote the corresponding point by 1_l and we study the trajectory of this point. Note that $Z(k_r) = j_l$, where $j = k + 2 \pmod 1$, $k = 1, 2, 3, 4$. There are two possibilities: either (i) $\widehat{\mathrm{SM}}(4_l) = 1_l$ or (ii) $\widehat{\mathrm{SM}}(4_r) = 1_l$. We consider case (i), the other case being similar. Since $\widehat{\mathrm{SM}}$ commutes with Z one has $\widehat{\mathrm{SM}}(2_r) = 3_r$, $\widehat{\mathrm{SM}}(2_l) = 3_l$ and $\widehat{\mathrm{SM}}(4_r) = 1_r$. There are two subcases: either (a) $\widehat{\mathrm{SM}}(1_l) = 2_l$ or (b) $\widehat{\mathrm{SM}}(1_l) = 2_r$. For the case (a), using again the fact that $\widehat{\mathrm{SM}}$ commutes with Z, one obtains $\widehat{\mathrm{SM}}(3_r) = 4_r$ and $\widehat{\mathrm{SM}}(3_l) = 4_l$. This implies that the trajectory is given by the iterates $\{1_l, 2_l, 3_l, 4_l, 1_l, ...\}$ and has period $\hat{p} = 4$. Similarly, for the case (b) one obtains $\widehat{\mathrm{SM}}(3_r) = 4_l$ and $\widehat{\mathrm{SM}}(3_l) = 4_r$. The corresponding trajectory is $\{1_l, 2_r, 3_r, 4_l, 1_l, ...\}$ which also has $\widehat{p} = 4$. □

On the other hand, the identification in terms of the central symmetry Z implies that $\widehat{p} = 4$ EPL trajectories on the figure-eight such that $\widehat{\mathrm{SM}}(1_l) = 3_l$ are also $p = 4$ trajectories, hence the SM trajectory have suffered a period-doubling bifurcation.

Summarizing, at the boundaries of the a-intervals of stability (generically) one observes that

- for $a_{tr=2}$ the SM trajectory undergoes a pitchfork bifurcation as it does the corresponding figure-eight DSM trajectory.
- for $a_{tr=-2}$ the SM trajectory undergoes a period-doubling bifurcation but there is a pitchfork bifurcation for the corresponding figure-eight DSM trajectory.

Finally, we note that the left pattern in Fig. 12 corresponds to values of k such that the two a-intervals do not overlap. See the comments after the proof of Theorem 2.1. The right pattern corresponds to the cases where there is overlap between the related a-intervals. The overlap is mainly expected for values of $|k| \leq b \log(2)$, this explains why for most of the continuations performed we observe the left pattern and not the right one.

Next, we comment on the abundance of $p = 2$ EPL for the STM and the related intervals of stability. For $\epsilon \in (0.7259590489256, 1.183026069380)$ we found a total amount of 223 different ϵ-intervals of EPL parameters. Each of the ϵ-intervals obtained by continuation corresponds to an a-interval in terms of the SM (2). The formal derivation of the SM for an *a priori stable* family F_ϵ (see [15, 19]) gives

$$a = a(\epsilon) = \frac{\log A(\epsilon)}{\log \lambda(\epsilon)} + \mathcal{O}\left(\frac{1}{\log \lambda(\epsilon)}\right), \tag{18}$$

where $A(\epsilon)$ denotes the width of the homoclinic lobes of the separatrices of the hyperbolic point H_ϵ with dominant eigenvalue $1 < \lambda(\epsilon) = \mathcal{O}(\epsilon^r)$, $r > 0$. For the STM (5) one has $\lambda(\epsilon) = 1 + \epsilon + \mathcal{O}(\epsilon^2)$ (i.e. $r = 1$), then $a(\epsilon) = \mathcal{O}(1/\epsilon^2)$ and the remainder in (18) is $\mathcal{O}(1/\epsilon)$.

For simplicity, we assume in the following that $a(\epsilon) = \log A(\epsilon)/\log \lambda(\epsilon)$, i.e. we ignore the remainder in (18) above (the effect of these ignored terms will be discussed later, see comments at the end of this section). Then, it is numerically easy to estimate $A(\epsilon)$ and $\lambda(\epsilon)$ for a given ϵ, and to approximate $a = a(\epsilon)$. In Fig. 14 left we represent, for each ϵ-interval of EPL parameters of the form (ϵ_1, ϵ_2), the value of the parameter $a = a(\epsilon_2)$. In the figure seven clouds of points with a similar form are distinguished (for values of $a \leq 7.3$ aprox.). Each cloud of points represents a

fundamental domain in terms of the a-parameter. From the SM theory one expects periodicity in the figure: changing a by $a+1$ the pattern of EPL must be repeated (this corresponds to crossing a fundamental domain). However, from the figure one observes that the pattern repeats for a increasing an amount ~ 0.8 instead of 1.

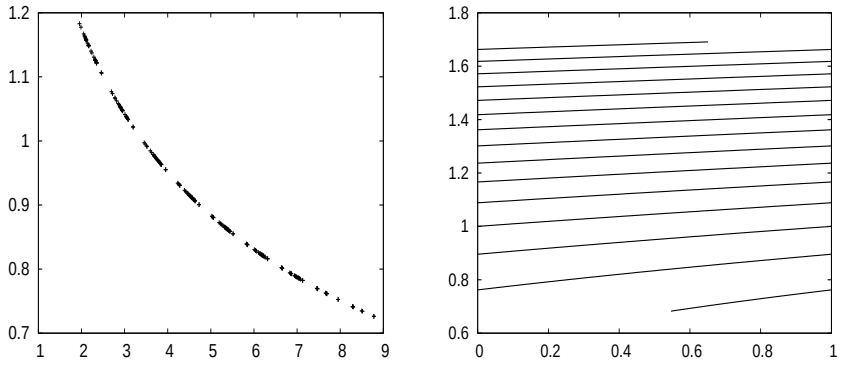

Figure 14: Left: Relation between the a of SM (2) and ϵ in STM (5). For each ϵ-interval (ϵ_1, ϵ_2) of EPL parameters we plot the point $(a(\epsilon_2), \epsilon_2)$. The parameter $\epsilon \in [0.7, 1.2]$ ranges in the vertical axis. The parameter a ranges on the x axis (it is not considered mod 1). Observe the periodicity in the figure: for each change of a by roughly 0.8 the distribution of the intervals is approximately repeated. Right: The (approximated) curve $\mathcal{C}$ that describe for the STM the parameters $(a(\epsilon), b(\epsilon))$ as $\epsilon \in [0.6, 1.6]$ varies. Here $a(\epsilon)$ is considered mod 1 and ranges in the horizontal axis, while $b(\epsilon)$ ranges on the vertical one. Compare with Fig. 3.

In Fig. 14 right we represent the curve $\mathcal{C}$ that describe $(a(\epsilon), b(\epsilon))$ as ϵ in the STM (5) varies. We have consider $\epsilon \in [0.6, 1.6]$ and $a(\epsilon)$ is considered mod 1. The curve has been obtained by a direct computation of the parameters $a(\epsilon) = \log A(\epsilon)/\log \lambda(\epsilon)$ and $b(\epsilon) = -\log \lambda(\epsilon)$ from the STM. Compare with Fig 3. Also note that the curve $\mathcal{C}$ becomes more transversal to the EPL strips of stability for values of $\epsilon \to 0$, see Fig. 8 left.

For the fundamental domains in Fig. 14 left, measured in terms of a, we computed the lengths of the related a-intervals, and removed the overlapping between them. That is, we computed the measure of the set E_b of a-EPL parameters of the related SM model (according to the notation in Section 1.4). We note that the parameter b is considered as fixed but depending on ϵ (formally speaking we estimate $m_L(E_{b(\epsilon)})$). The corresponding results, obtained directly from the STM computations, are summarized in Table 3. We observe that the values behave quite regularly even for the range of ϵ considered, which still quite far from the limit $\epsilon = 0$ (Fig. 6 right shows a similar behavior).

a-interval	$m_L(E_{b(\epsilon)})$
$[2.5, 3.3]$	0.06619105
$[3.3, 4.1]$	0.07210729
$[4.1, 4.9]$	0.06797864
$[4.9, 5.7]$	0.07159551
$[5.7, 6.5]$	0.08013797
$[6.5, 7.3]$	0.07146606

Table 3: Measure of the set of a-EPL parameters for the STM (5).

From Theorem 2.2 one expects $m_L(E_b) \approx 0.045$. However, the values in Table 3 exceed the predicted value by a factor (roughly) between 1.5 and 1.8. Note that our theoretical result concerns the limit $\epsilon \to 0$ while $\epsilon \in [0.7, 1.2]$ in our numerical investigations. The following (ignored) effects could explain why it is observed such a difference between the theoretically expected values and the direct computations.

- The SM (2) only considers the first harmonic of the oscillation between $W^{u/s}_{loc}(H_\epsilon)$ (see comments in Section 1.3) which is the dominant one for values of $\epsilon \to 0$. However, we have considered quite large values of ϵ in the previous example and we can not guarantee that the effect of the ignored harmonics is small enough. A higher order SM model could be useful in this context.

- Both parameters a and b depend on ϵ. As ϵ changes they describe a curve $\mathcal{C}$ in the (a, b)-plane ($b(a) \approx \epsilon^r a$, for suitable $r > 0$, see Fig. 3). On the other hand, the slope of the strips of stability tends to $1/\log(2)$ as $\epsilon \to 0$ (see Fig. 8). Accordingly, one expects a periodicity in a with period $\approx 1 + \mathcal{O}(\epsilon^r)$ instead of 1. Taking this effect into account, however, the values in Table 3 differ even more from the theoretically expected ones.

- The relation between ϵ and a is given by (18) and we have ignored terms $\mathcal{O}(1/\epsilon)$. The dominant term of the ignored ones can be computed using the natural parameterization of the unperturbed separatrices (given by the pendulum and depending on $\epsilon > 0$), see [15, 22]. This dominant ignored term of $\mathcal{O}(1/\epsilon)$ produces a relative error in a of order $\mathcal{O}(\epsilon)$. For the range of ϵ values considered, this effect can be large. Moreover, the higher order ignored terms can also play a role. Again, an analysis of a higher order SM model could predict values closer to the observed ones.

To sum up, the theoretical approach of Section 2 has allowed us to give a complete qualitative description of the set of $p = 2$ EPL parameters for the STM (5), predicting the bifurcations, the periodicity and even the overlapping of the a-intervals of stability. On the other hand, we have shown the limits of the SM model (2) to get quantitative results for "realistic" ϵ values relatively far from the limit $\epsilon \to 0$.

4 Stability islands visiting homoclinic lobes for the $1:4$ resonance of the Hénon map

Section 2 was devoted to study the abundance of EPL using the SM model (2). We concluded that for a one-parameter family of close-to-integrable maps we expect to have islands visiting homoclinic lobes for, approximately, the 5% of the parameter values. The results in Section 3 are in (relatively) good agreement with such a prediction for the STM family (5).

At this point, one can ask whether the separatrix model applies in a "real" situation, that is, for a given map inside the homoclinic lobes of a given resonance. From a theoretical point of view this is far beyond our capabilities: as observed in [19] it can be very hard to effectively determine which is the validity domain of the separatrix model when applied to a concrete system. From a practical point of view note that, to relate the map with the model, the parameters of the last one should be determined, at least numerically, according to the real dynamics. This turns out to be not a simple task, see comments in Section 3 on the STM, which certainly requires more attention due to the interest in many applications. Moreover, the proper model will be

the DSM (1) instead (that is without central symmetry, see [19]) but this is a minor difficulty once it is known how to proceed.

The previous considerations on EPL trajectories for the SM and the STM also reveal us their bifurcation pattern. A simple question concerns the genericity of this pattern and the possibility to observe it in a given generic (without central symmetry) family of APMs. To this end, we consider the Hénon map (6). Concretely, we focus on the fourth order resonant islands arising for $c > 1$ (see Fig. 15 left). We recall from [18] that the inner splitting for this resonant chain of islands is almost negligible. Hence, we look for periodic orbits (p.o.) visiting the outer homoclinic lobes (see Fig. 15 right).

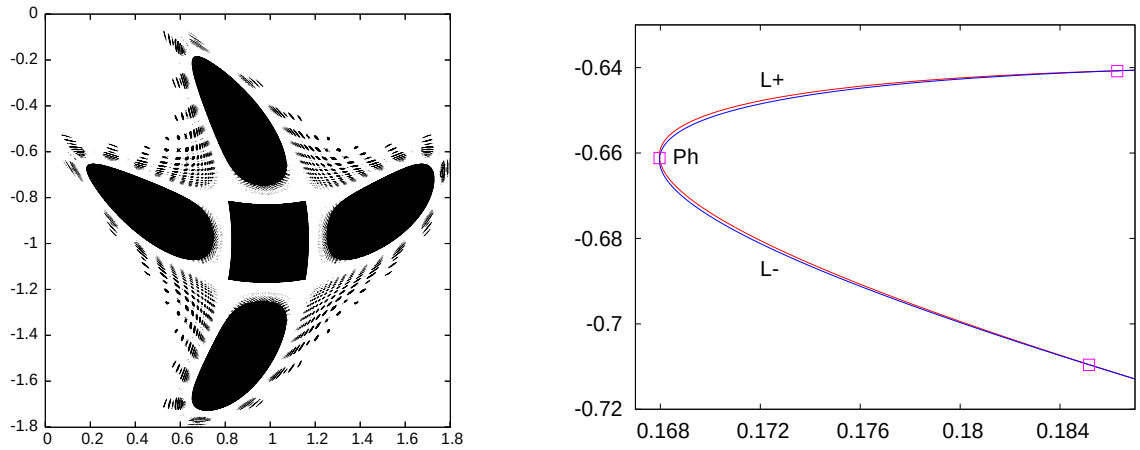

Figure 15: Map (6), $c = 1.015$. The left plot shows the period-4 islands that have been detached from the central component of the stability domain around the fixed point, and many satellite islands. The right plot shows the invariant manifolds related to the 4-periodic hyperbolic orbit. They form the homoclinic lobes L_+ and L_-. It corresponds to a magnification of the segments of the separatrices surrounding one of the islands (the left one) whose elliptic point is on the parabola $c(x^2-1)/2 - x$.

One is tempted to look directly for p.o. by scanning systematically points inside a homoclinic lobe but this is a fruitless way to proceed with many numerical inconveniences, due to the tiny size of the islands. A better option is to take advantage of the symmetries of the Hénon map to perform more accurate computations. The Hénon map (6) is reversible with respect to $R : y = -x$ and with respect to the parabola $Q_1 : y = g_{Q_1}(x) = c(x^2-1)/2 - x$. The corresponding reversors are $S_R : (x, y) \mapsto (-y, -x)$ and $S_{Q_1} : (x, y) \mapsto (x, c(x^2-1) - 2x - y)$ respectively. In what follows Q_2 will denote the parabola $Q_2 = H_c(Q_1) = S_R(Q_1)$.

Instead of looking for all possible p.o. we restrict ourselves to p.o. of the following type. Consider the 1:4 resonant island $\mathcal{I}_1$ having the elliptic point on Q_1 for $x < 1$ (see Fig. 16). Note that there is an outer homoclinic point p_h, related to a transversal intersection of the invariant manifolds bounding this island, located on Q_1, as can be also seen in Fig. 15, right. The manifolds come from the hyperbolic periodic orbit whose points are h_1, h_2, h_3, h_4. Denote by L_+ and L_- the two lobes adjacent to p_h, formed by the outer separatrices of this island, which are located above and below Q_1 respectively (see Fig. 15 right and Fig. 16). Then we look for p.o. that, under iteration by the current map, H_c^4, describe the following path (the notation in the following description refers to Fig. 16, which is an example of the type of orbits we consider):

Starting with an initial point $q \in \mathcal{I}_1$ on Q_1 close to the inner separatrices this point is mapped,

after passing close to h_1 under some iterates, to the lobe L_-. Then, it "goes outside the island $\mathcal{I}_1$", that is, under iteration it passes close to the 4-periodic point h_2 and then "surrounds" the island $\mathcal{I}_2$. When coming close to h_3, it turns to the left, that is, the iterates go towards the parabola Q_2. Finally, after a suitable number of iterates we require the point to be on Q_2.

The required condition is transcribed as $H_c^{4m}(q) \in Q_2$ for some $m \in \mathbb{N}$. It is equivalent to $H_c^{4m-1}(q) \in Q_1$. The total period of the orbit is then $8m-2$. Note that it implies that a suitable H_c^4-iterate of q has to fall into the lobe $H_c^{-1}(L_+)$ in $\mathcal{I}_2$ (otherwise the iterates will not go towards Q_2 when passing close to h_3). The symmetries of the Hénon map imply that the lobe $H_c^4(H_c^{-1}(L_+))$ is located on the right side of Q_2 in the lower outer part of the island $\mathcal{I}_2$. That is, the outer homoclinic point on Q_2 related to the manifolds bounding $\mathcal{I}_2$ does not belong to the orbit of the homoclinic point p_h.

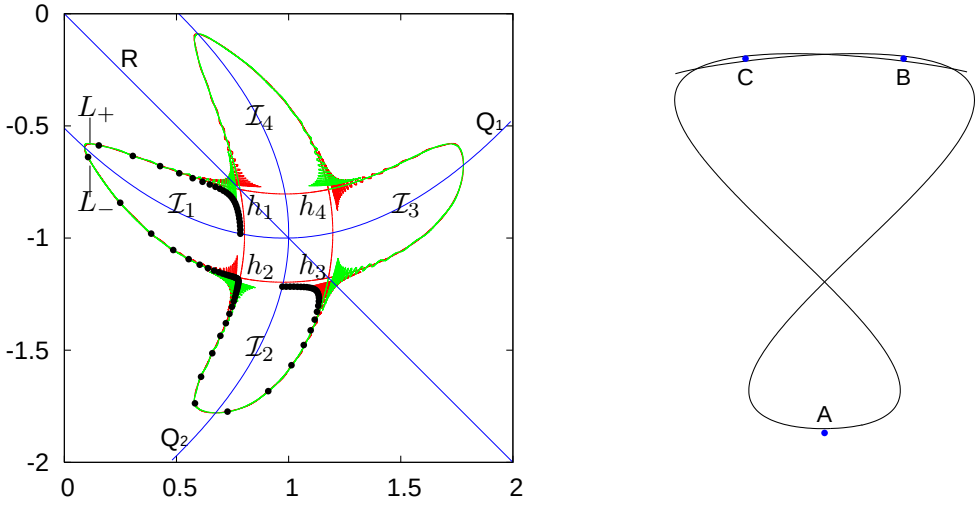

Figure 16: Left: Example of the type of symmetric periodic orbits considered. The black dots correspond to iterates by H_c^4, with $c = 1.02$, of the initial point on the parabola Q_1 with $x \approx 0.78481059138432541$. After $m = 93$ iterates of H_c^4, exactly the ones depicted in the figure, the orbit is on $Q_2 \cap \mathcal{I}_2$. Equivalently, under H_c^{371} the orbit is on $Q_1 \cap \mathcal{I}_3$. The periodic orbit has period $P = 742$. Moreover, $Trace(DH_c^{742}(x,y)) \approx 6.9657 \times 10^6$, where $y = g_{Q_1}(x)$. Right: a schematic representation of the kind of orbits (see text).

To numerically illustrate the existence and the pattern of the stable p.o. we choose $c = 1.02$ in (6). This value is chosen because there are not r.i.c. outside the $1:4$ resonant chain, a fact that helps in numerical computations since points are able to escape to infinity (see comments in Section 4.1.1). On the other hand, the $1:4$ resonance is created at $c = 1$, hence for values of c closer to 1 the computations require an increase in the number of digits in the high precision arithmetic.

Scanning for p.o. of the type explained taking $c = 1.02$ we found a set PO of 274896 p.o. with total period P less than 1200. All of them are highly hyperbolic, the traces of the differential matrix on them having an order of magnitude ranging from 10^4 to 10^{18} (we have used double precision arithmetic in this rough scanning process). We consider the subset $PO_{<10^8}$ of p.o. of PO such that the trace of the differential matrix at the p.o. is less than 10^8. It turns out that $\#PO_{<10^8} = 2367$.

The mechanism of creation of these orbits when the parameter evolves can be explained geometrically in terms of the dynamics of the homoclinic lobes created by the invariant manifolds

bounding the resonant 4-islands (see details in the paragraph below). In particular, the orbits in PO are born, as usual, in a saddle-center (SC) bifurcation at some value c_{sc} depending on the orbit. For $c = c_{sc}$ the trace of differential at the bifurcating point is equal to 2. After the saddle-center bifurcation the elliptic orbit may suffer a period-doubling (PD) bifurcation and becomes reflexive hyperbolic or a pitchfork (PF) and becomes hyperbolic. This will happen if the rotation number at the elliptic point changes in a continuous quick way when moving the parameter. Note that this is the reason why all the orbits found are highly hyperbolic. Then, by continuation of all the p.o. in $PO_{<10^8}$, we find the intervals of the parameter c for which there are EPL. These intervals will be referred as c-intervals of stability.

To look for these c-intervals of stability we restrict the continuation to values of c in the interval $I_{cont} = [c_m, c_M] = [1.0198, 1.02]$. This is enough because it is, in some sense, a fundamental interval in what concerns the parameter: for smaller values, the pattern is repeated as we comment at the end of this paragraph. As said, this can be explained in terms of lobe dynamics, as a consequence of the well-known λ-lemma. We recall that in order to have a p.o. of the type we look for, it is required that some H_c^4-iterate of the initial point on Q_1 belongs to the lobe $H_c^{-1}(L_+)$ and then "it has to go inside" $\mathcal{I}_2$ at the corresponding passage close to h_3. Denote by l_k the k-th iterate of the lobe $H_c^{-1}(L_+)$ under H_c^4. For a p.o. of the considered type there must exist $k_0 = k_0(c)$ such that for $k \geq k_0$ the lobe l_k intersects the parabola Q_2 close to the inner separatrices bounding $\mathcal{I}_2$. When decreasing c along the interval I_{cont} the lobe l_{k_0} moves. Consequently, there exists $c_0 \in I_{cont}$ such that for $c < c_0$ one has $k_0(c) = k_0(c_M) + 1$. For decreasing c, when $c = c_0$ the p.o. of lower possible period are destroyed in a saddle-center bifurcation. For $c < c_0$ the geometrical situation repeats again for the lobe l_{k_0+1} and the subsequent lobes. It is in this sense that the interval considered is a fundamental interval.

The continuation shows that for a given p.o. in $PO_{<10^8}$ there are at most two c-intervals of stability (for $c \in I_{cont}$). In other words, for values of c in those intervals the p.o. considered is elliptic (we remark that there is no general reason to expect at most two c-intervals of stability, despite they can be found in some normal forms if we accept that they are valid even far away from the sc bifurcation). Define $\hat{c} = 1.02 - c$. The Fig. 17 shows the behavior of the trace with respect to the $\hat{c}$ parameter. We observe that, following the lower part of the curve, the elliptic point becomes reflexive hyperbolic, then elliptic again and finally hyperbolic. This is the pattern observed for all the computed orbits in $PO_{<10^8}$. Note that the absence of central symmetry allows for period-doubling bifurcation of the EPL trajectory (compare with the STM case in Section 3). In particular, the set of p.o. obtained for $c = 1.02$ are organized by pairs, according to the saddle-center bifurcation where they are created, having c-intervals of stability with the same pattern.

Performing the continuation for all the p.o. of $PO_{<10^8}$ we obtain 1989 different c-intervals of stability. The sum of the lengths gives $\approx 7.216 \times 10^{-8}$. However, there is one pair of intervals overlapping each other, the length of the overlapping c-interval being $\approx 7.82 \times 10^{-12}$. All the c-intervals observed are contained in the interval $I_c = [1.0198002517482521, 1.02]$, of total length $1.99748251747955 \times 10^{-4}$. Hence, the fraction of parameter values $c \in I_c$ for which EPL exist is $\approx 3.61 \times 10^{-4}$. Moreover, the largest c-interval of stability observed has length $\approx 0.82 \times 10^{-9}$, while the length of the computed smallest one is $\approx 2.1 \times 10^{-20}$. The largest gap in I_c without detected stability intervals has length $\approx 0.2549167177 \times 10^{-5}$.

We should note that the result obtained does not quantitatively agree with the previously obtained for the SM in Theorem 2.1, but the reader should take into account the following specific considerations.

- The type of EPL trajectories considered for the Hénon map is not of the type considered

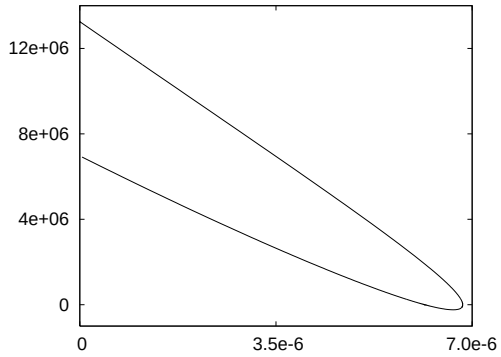

Figure 17: The stability c-intervals obtained by continuation (restricted to $c \in I_{cont}$) of the p.o. shown in Fig. 16. In the horizontal (resp. vertical) axis we display $\hat{c} = 1.02 - c$ (resp. $Trace(DH_c^{742}(x,y))$, where $y = g_{Q_1}(x)$, for the corresponding c value). The continuation provides two c-intervals of stability. The left one, $\hat{c} \approx (6.83146655146675 \times 10^{-6}) \pm (-5.95 \times 10^{-18})$, contains the saddle-center bifurcation and it is the smallest of the two. The other interval, the largest one, is $\hat{c} \approx (6.155133825 \times 10^{-6}) \pm (-2.835 \times 10^{-12})$.

for the SM results (see Fig. 16). If on Fig. 16 left we identify the four loops around the period-4 islands and, hence, all the points $h_j, j = 1, 4$ according to the topology of the figure-eight representation (see [19]) it turns out that the orbits considered can be seen as the period $\hat{p} = 3$ EPL studied in [17], as illustrated in Fig. 16 right. The initial point A is mapped to B, then to C and then back to A. The point A can be identified to the initial point q for the Hénon map, and then points B, C as points on the lobes L_-, L_+, respectively. Moreover, the central symmetry does not hold for the situation studied.

- The symmetries of the Hénon map also play a role since they should be respected by the p.o. On the other hand, we have only considered a specific type of p.o. and the total number of EPL is expected to be much larger. Note, for example, that the two elliptic p.o. created in the PD bifurcation (2) or in the PF bifurcation (4) in Fig. 18 are not of the type considered since they are not on the parabola Q_1 (see details below). Moreover, the SM results of Section 2 concern the limit when approaching to integrable (i.e. $b \to \infty$) which would be equivalent to $c \to 1$ and we have chosen values of c far still relatively from this limit ($c \approx 1.02$).

- A final consideration which could explain the difference of the results obtained from the separatrix map and the $1:4$ resonance of the Hénon map refers to the fact that a proper model to describe the dynamics within the lobes of the $1:4$ resonant islands is not the separatrix map SM (2) but the double separatrix map DSM (1). The parameters of the DSM model, $a_{s,\bar{s}}, \nu_{\bar{s}}$ and b, change as the parameter c in (6) changes. Similarly to the separatrix map case studied in the last section, one expects the total number of periodic orbits inside the lobes of the $1:4$ resonant island to depend on the concrete way the parameters of the model DSM change as c evolves. A priori we do not know if this dependence is like the shown in Fig. 3 for $p = 2$ EPL trajectories of the SM.

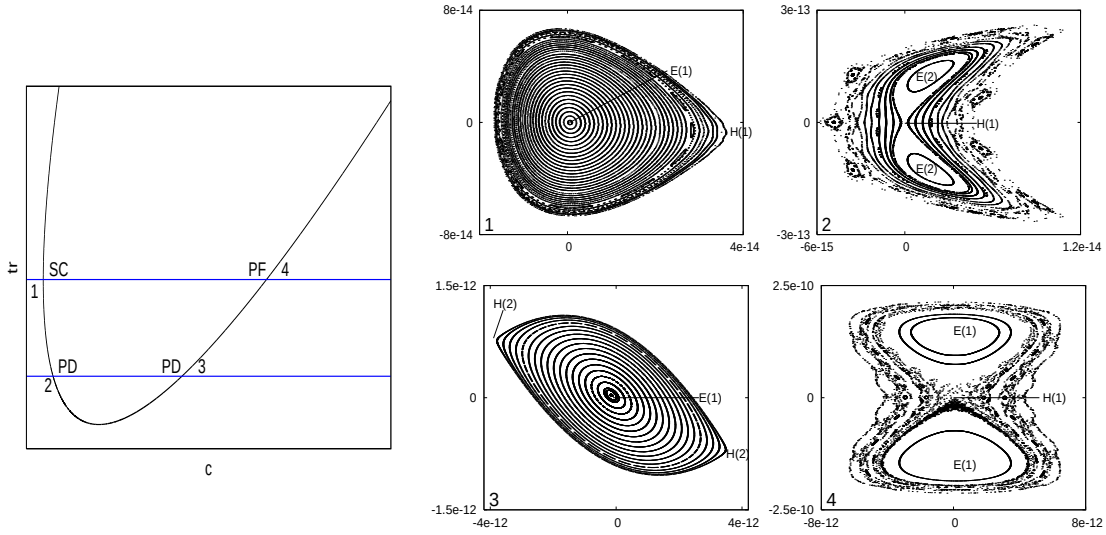

Figure 18: Schematic representation (left, only qualitative) of the trace vs. the parameter c in an orbit of the type considered. The numbers 1 to 4 refer to the ones shown in the left lower corner of the right plots. The codes SC, PD and PF mean saddle-center, period-doubling and pitchfork. The right plots correspond to the period $P = 742$ EPL trajectory of the previous figures. The elliptic (E) and hyperbolic (H) points are shown. In parenthesis, (1) or (2), it is shown the period of the point under H_c^{742}. The values of $\hat{c}$ used in the right plots are taken slightly greater than, but very close to, the values of c at the bifurcations.

4.1 Some comments on the relevance of EPL in the phase space

Our next goal is to illustrate the islands of stability we have been discussing about. As explained before, the continuation of the p.o. considered determines two c-intervals of stability. The smallest one is the one which ends up at the saddle-center bifurcation. The different bifurcations suffered when leaving the c-intervals of stability are shown in Fig. 18, where the plotted islands correspond to the previously considered $P = 742$ EPL. Similar patterns are found for all the orbits computed. Note that the c values are taken very close to the bifurcations.

At the center of the c-intervals of stability the islands are not so small as the ones shown in Fig. 18. To show a larger island (of smaller period, as it can be expected) take, for instance, $\hat{c} = 3.6491792 \times 10^{-6} := \hat{c}^*$. For this value of the parameter there is an elliptic p.o. of the type considered, located at $x \approx 0.7932840705714759$ with period $P = 678$. This orbit is created at the SC bifurcation which happens for $\hat{c} = \hat{c}_{bif} \approx 3.64917922 \times 10^{-6}$ as shown in Fig. 19 left.

In Fig. 19 right we show a relatively large stability island which corresponds to one of the orbits on the left plot in the small stability range. In that case this c-interval of stability has length 7×10^{-13} approximately. As always found in the present example, there is a larger c-interval of stability of length $\approx 7.346 \times 10^{-10}$. In Fig. 20 we show the evolution of the island of stability in this larger interval of c. We observe the typical evolution pattern of an island when changing the rotation number at the elliptic point. Note that the island of stability subsists for a while, as it should be, when the elliptic central point has suffered a pitchfork bifurcation.

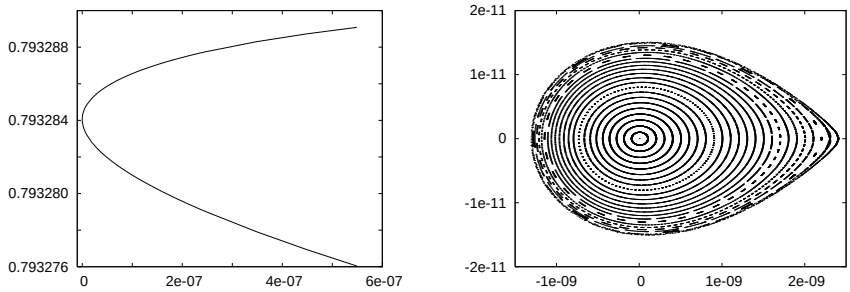

Figure 19: Left: In the horizontal axis $c - c_{bif}$, with $c_{bif} = 1.01999635082078$ is shown. In the vertical one, we represent the value of the x-coordinate of the periodic orbit located on the parabola Q_1 in the left part of the $1:4$ resonance for the map (6) for period 678. Right: The corresponding island of stability for $c - c_{bif} = 2 \times 10^{-14}$. The periodic point has been moved to the origin and the Q_1 curve has been taken as horizontal axis.

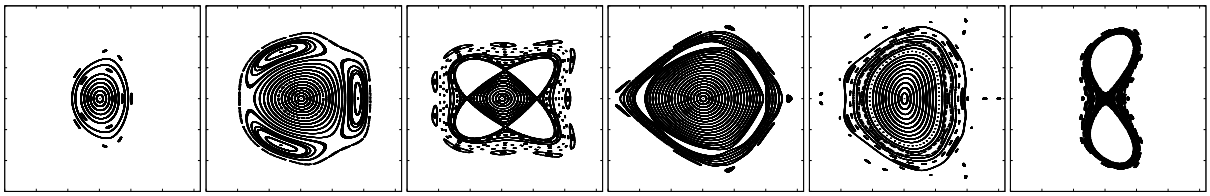

Figure 20: Islands of stability within the large interval of stability obtained by continuation of the orbit shown in 19 right. The values of $\hat{c}$ are of the form $\hat{c} = \eta \times 10^{-6}$ and, from left to right, $\eta = 3.51015$, 3.51, 3.50985, 3.5097, 3.50955 and 3.50945. We show the island of stability on Q_1. The coordinates are adapted to put the origin at the elliptic 678-periodic point and the parabola Q_1 as the horizontal axis. The width of all the windows shown is 3×10^{-10} and the height 3×10^{-6}. They give an idea of the size of the islands.

4.1.1 Some statistics of the escaping orbits

Finally, to end this section, we perform the following numerical experiment. For the value $\hat{c} = \hat{c}^*$ we have on Q_1 the island shown in Fig. 19 right. As detailed in [19] there are many chains of islands surrounding the period 4 island of H_c (the situation is similar to the one in Fig. 15 left). We take an arc in the line Q_1 between the end of these islands and the separatrix going from h_1 to h_2 and scan it with respect to x (see Fig. 16). All points escape except a couple of hundreds which sit in tiny islands. The idea is to study how these points escape under iterations of H_c (we note that there is no r.i.c. surrounding the $1:4$ resonant islands for this value of c). An escape is easy to identify: the iterates approaching to the hyperbolic fixed point on $(-1, 1)$ close to the left branch of W^u go to infinity. The number of iterates to escape depends strongly on the initial point and on the value of c. Similar computations have been done for different c values. The Fig. 21 shows a sample of results. The values of c in the plot, from left to right, are $c_1 = 1.06$, $c_2 = 1.04$, $c_3 = 1.0199964903$, which corresponds to the value of c for which we have one of the largest island in the largest c-interval of stability (4th plot in Fig. 20) and $c_4 = 1.02 - \hat{c}^*$. The step in x is always 10^{-9}. The number of scanned points is roughly (in millions of initial points) 435, 294, 53.4 and 98.5 for $c_i, i = 1, \ldots, 4$. A maximal number of 10^8 iterations has been used for each initial point. The average number of iterations under H_c to escape takes the approximate values 92, 414, 38000 and 46000 for the four values of c.

The Fig. 21 shows the number of points $r(m)$ which remain before escape as a function of the number of iterates m, using $\log_{10}$ to display both variables. The few points which do not escape (of the order of 10^6 of the total) are not counted in the plot. The orbits look, in some sense, like a random walk before escaping. In a pure diffusive regime, assuming existence of absorbing barriers, even with different diffusion coefficients bounded from above and below, we expect an exponential decay $r(m) = \exp(-\alpha m)$, with α a positive constant [7]. Due to the stickiness of the chains of islands and to the existence of Aubry-Mather sets with "narrow gaps", diffusion is slowed down, as if the diffusion coefficient approaches zero. The increasing average number of iterates and the plot reflect this effect. Furthermore the plot shows ranges of m where the dominant character is an exponential decrease, with other with an inverse power behavior. These questions will be studied in forthcoming works, like [20]. As far as the authors know there are few works studying systematically the ratio of diffusion across chaotic zones of APM, the celebrated papers [4, 5] being the most relevant exceptions.

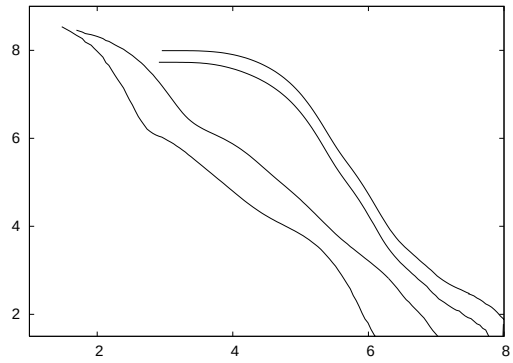

Figure 21: Number of points that escape under m iterates of H_c, depending on the value of c. In the horizontal variable we display $\log_{10}(m)$. In the vertical axis it is shown $\log_{10}(r(m))$, being $r(m)$ the number of points that do not escape in m iterates. See text for details and for the concrete values of c used.

5 Conclusions and future work

We have shown the abundance of $p = 2$ EPL for the SM lobes and for the lobes related to the hyperbolic point of the STM. Also we have studied the abundance of an specific type of EPL visiting the lobes related to the $1:4$ resonant island of the Hénon map. In all cases a relative amount of EPL have been found, in agreement with the results in [17].

To conclude with, we list some open questions that this work suggests:

- We have estimated a lower bound $m_L(E_b)$ for the SM in terms of the subset of EPL from $E_b^{\{4\}}$, but the real value of this measure remains unknown. We believe that EPL with higher period p will not change the final value significantly.
- For general families F_ϵ, like the Hénon map or the STM, the parameters a and b are related as described (3). This gives a curve $\mathcal{C}$ in the (a, b)-plane. How this curve behaves for EPL visiting the lobes of a generic $(p:q)$ resonance of a family of APMs? On the other hand, we have approximated this curve for the STM but the proper curve depends on a higher order SM model.

- Concerning the bifurcations of the EPL visiting the lobes of the $1:4$ islands of the Hénon map (Fig. 18) the corresponding cascades of bifurcations should be investigated. Different patterns seem to be possible.

Acknowledgments

This work has been supported by grants MTM2006-05849/Consolider (Spain), MTM2010-16425 (Spain) and 2009 SGR 67 (Catalonia). The authors are indebted to D.V. Treschev and A.I. Neishtadt.

References

[1] I. Baldomà and E. Fontich. *Exponentially Small Splitting of Invariant Manifolds of Parabolic Points*, volume 167 of *Memoirs of the American Mathematical Society*. American Mathematical Society, 2004.

[2] H. Broer, C. Simó, and J.C. Tatjer. Towards global models near homoclinic tangencies of dissipative diffeomorphisms. *Nonlinearity*, 11:667 – 770, 1998.

[3] L. Chierchia and G. Gallavotti. Drift and diffusion in phase space. *Annales de l'I.H.P.*, 60:1–144, 1994.

[4] B.V. Chirikov. A universal instability of many-dimensional oscillator system. *Phys. Rep.*, 52:264 – 379, 1979.

[5] B.V. Chirikov. Chaotic dynamics in Hamiltonian systems with divided phase space. In *Proceedings of the Sitges Conference on Statistical Mechanics*, volume 179, pages 29 – 46. Springer-Verlag, 1983. Lecture Notes in Physics. Dynamical Systems and Chaos.

[6] G. Contopoulos, E. Grousouzakou, and C. Polymilis. Distribution of Periodic Orbits and the Homoclinic Tangle. *Celestial Mechanics and Dynamical Astronomy*, 64:363–381, 1996.

[7] W. Feller. *An introduction to probability theory and its applications*, volume I – II. John Wiley & Sons Inc., New York, N.Y., 1950–1966.

[8] L. Kuznesov and G.M. Zaslavsky. Hidden renormalization group for the near-separatrix hamiltonian dynamics. *Phys. Rep.*, 288:457–485, 1997.

[9] L. Kuznesov and G.M. Zaslavsky. Scaling invariance of the homoclinic tangle. *Phys. Rev. E*, 66:1–7, 2002.

[10] A. Neishtadt, V. Sidorenko, and D. Treschev. Stable periodic motions in the problem on passage through a separatrix. *Chaos*, 7(1):2–11, 1997.

[11] A. Neishtadt, C. Simó, D. Treschev, and A. Vasiliev. Periodic orbits and stability islands in chaotic seas created by separatrix crossings in slow-fast systems. *Discrete Contin. Dyn. Syst. Ser. B*, 10(2-3):621–650, 2008.

[12] A. Neishtadt, C. Simó, and A. Vasiliev. Geometrical and statistical properties induced by separatrix crossings in volume-preserving systems. *Nonlinearity*, 16(2):521–557, 2002.

[13] A. Neishtadt and A. Vasiliev. On the absence of stable periodic orbits in domains of separatrix crossings in nonsymmetric slow-fast Hamiltonian systems. *Chaos*, 17(4):043104, 7, 2007.

[14] A. Neishtadt, A. Vasiliev, C. Simó, and D. Treschev. Stability islands in domains of separatrix crossings in slow-fast hamiltonian systems. *Proceedings of the Steklov Institute of Mathematics*, 259:236–247, 2007.

[15] G.N. Piftankin and D.V. Treschev. Separatrix maps in Hamiltonian systems. *Russian Math. Surveys IOP*, 2(62):219–322, 2007.

[16] C. Simó and D.V. Treschev. Evolution of the "last" invariant curve in a family of area preserving maps. http://www.maia.ub.es/dsg/2006/index.html.

[17] C. Simó and D.V. Treschev. Stability islands in the vicinity of separatrices of near-integrable maps. *Discrete Contin. Dyn. Syst. Ser. B*, 10(2-3):681–698, 2008.

[18] C. Simó and A. Vieiro. Resonant zones, inner and outer splittings in generic and low order resonances of area preserving maps. *Nonlinearity*, 22(5):1191–1245, 2009.

[19] C. Simó and A. Vieiro. Dynamics in chaotic zones of area preserving maps: close to separatrix and global instability zones. *Physica D*, 240(8):732–753, 2011.

[20] C. Simó and A. Vieiro. Dynamical description of the domain of stability of area preserving maps. Work in progress, 2011.

[21] The PARI Group, Bordeaux. *PARI/GP, version* `2.3.4`, 2008. available from http://pari.math.u-bordeaux.fr/.

[22] D. Treschev and O. Zubelevich. *Introduction to the perturbation theory of Hamiltonian systems*. Springer Monographs in Mathematics. Springer-Verlag, 2010.

[23] R.B. White and G.M. Zaslavsky. Near threshold anomalous transport in the standard map. *Chaos*, 8(4):758–767, 1998.

[24] G.M. Zaslavsky. Dynamical traps. *Phys. D*, 168–169:292–304, 2002.

[25] G.M. Zaslavsky and N.N. Filonenko. Stochastic instability of trapped particles and conditions of applicability of the quasi-linear approximation. *Soviet Physics JETP*, 27:851–857, 1968.